Intermediate and deep ocean current circulation in the Mozambique Channel: New insights from ferromanganese crust Nd isotopes

Claire Charles, Ewan Pelleter, Sidonie Révillon, Philippe Nonnotte, Stephan J. Jorry, Jean-Michel Kluska

Intermediate and deep ocean current circulation in the Mozambique Channel: new insights from ferromanganese crust Nd isotopes

Claire Charles [a, b], Ewan Pelleter [a], Sidonie Révillon [b, c], Philippe Nonnotte [b], Stephan J. Jorry [a], Jean-Michel Kluska [d]

[a] IFREMER, Unité Géosciences Marines, Laboratoire Cycles Géochimiques (LCG), F-29280 Plouzané, France

[b] Univ Brest, CNRS, UMR 6538 (Laboratoire Géosciences Océan), Institut Universitaire Européen de la Mer (IUEM), Place Nicolas Copernic, 29280 Plouzané, France

[c] SEDISOR/UMR 6538 (Laboratoire Géosciences Océan), Institut Universitaire Européen de la Mer (IUEM), Place Nicolas Copernic, F-29280 Plouzané, France

[d] TOTAL Exploration and Production, CSTJF, Avenue Larribau, F-64000, Pau, France

Corresponding author :

claire.charles@ifremer.fr

Abstract

The Mozambique Channel plays a key role in the exchange of water masses between the Indian and Atlantic Oceans, which include the North Atlantic Deep Water (NADW) inflow from the south and the North Indian Deep Water (NIDW), an aged form of the NADW spreading poleward from the northern and equatorial Indian Ocean basin. Several authors assume that the Davie Ridge acts as a topographic barrier to the northward advection of NADW, which would therefore be absent in the Comoros Basin. Other studies suggest that the NADW flows from the south of the Mozambique Channel to the Comoros Basin, indicating that the Davie Ridge may not currently constitute a blocking topographic barrier to deep water mass circulation. To address this question, we studied ferromanganese (Fe, Mn) crusts collected over 2000 kilometres in the Mozambique Channel, from the Agulhas Plateau to the Glorieuses Islands. Neodymium (Nd) isotope compositions (ε_{Nd}) of surface scrapings range between ε_{Nd} = -10.1 above the Agulhas Plateau, which might reflect the NADW inflow, and more radiogenic values between ε_{Nd} = -8.0 and -8.2 in the Glorieuses area, highlighting the NIDW influence. However, value of ε_{Nd} = -9.4 measured north of the Davie Ridge cannot be explained by the sole influence of the NIDW and therefore highlights the advection of the NADW northeast of the Comoros Basin. We estimate that the contribution of the NADW through the channel is up to 68% in the Agulhas Plateau and 60% north of the Davie Ridge. These findings are consistent with previous hydrographic studies and suggest that the Davie Ridge does not currently act as topographic barrier to deep currents.

Keywords

Ferromanganese crusts

Nd isotopes

Paleoceanography

Mozambique Channel

North Atlantic Deep Water

1. Introduction

Ferromanganese crusts (Fe, Mn) are marine deposits that are ubiquitous on the seafloor i.e. occur in diverse environments and at different depths. They precipitate directly from seawater on hard substrates (Hein et al., 2009) and their growth rate can vary between 0.5 and 15 mm/Ma according to the geodynamic and paleogeographic context (Kusakabe and Ku, 1984; Segl et al., 1984; Eisenhauer et al., 1992; Frank et al., 1999). As a result, the thickest crusts may represent time intervals up to 80 Ma (Frank et al., 1999). This very low precipitation rate, coupled with the fact that Fe and Mn oxyhydroxides are significant element scavengers (e.g. metals, trace elements, rare earth elements (REE); Piper, 1974; Hein et al., 2010; Lusty et al., 2018), results over time in extensive enrichment of seawater elements in the Fe-Mn crusts. These crusts therefore contain records of element cycles in the oceans (Aplin and Cronan, 1985) with each millimeter of thickness corresponding to a specific time period. They constitute ocean archives, studied since the 1980s to understand the biogeochemical cycles of metals (Koschinsky and Halbach, 1995; Koschinsky et al., 1997), and more recently, to trace global ocean current flow paths (Albarède and Goldstein, 1992; Albarède et al., 1997; Christensen et al., 1997; Frank et al., 1999). Several authors have focused on multi-element and isotopic compositions of Fe-Mn crusts from the Atlantic, Indian and Pacific Oceans. Their neodymium (Nd) isotope compositions (ε_{Nd}) have been particularly assessed (Aplin et al., 1986, Albarède et al., 1997, 1998; Frank et al., 1999). These previous global-scale studies have established the current average geochemical compositions of seawater for each geographic oceanic basin and identified major geodynamic, geochemical and climate changes over the past 15 Ma (Segl et al., 1984; Christensen et al., 1997; Ling et al., 1997; Frank, O'nions, 1998; O'nions et al., 1998; Frank et al., 1999; Frank et al., 2002; Hein et al., 2016). However, few analyses have been made on Fe-Mn crusts on local scale in mixing areas such

as the Mozambique Channel, a strategic zone for studying the Atlantic and Indian water mass mixing (You, 2000; de Ruijter et al., 2002; van Aken et al., 2004; Collins et al., 2016; Fig. 1).

The circulation of deep currents is widely described due to the Davie Ridge (Coffin and Rabinowitz, 1987) that separates the channel into two distinct basins (i.e. the Comoros Basin in the north and the Mozambique Basin in the south; Fig. 1). According to some authors, the Davie Ridge represents a topographic obstacle to the circulation of these deep currents flowing from the Atlantic Ocean to the south and from the Indian Ocean to the north (Toole and Warren, 1993; Mantyla and Reid, 1995; You, 2000; Fig. 1B). However, recent hydrographic data have identified deep currents from the Atlantic Ocean north of the Davie Ridge (DiMarco et al., 2002; van Aken et al., 2004; Collins et al., 2016), and thus called into question the evolution of deep currents in the Mozambique Channel as well as the role of the Davie Ridge in the distribution of these water masses.

In this study, we analyzed the Nd isotope composition of 29 crusts collected through the Mozambique Channel in order to better understand the oceanic processes in the study area. The main objectives of this paper are to (1) identify deep water masses circulation (2) interpret the actual impact of the Davie Ridge on water mass propagation to the north and (3) propose new hydrographic framework of the deep currents in the Mozambique Channel. This is the first time that such a detailed study in terms of the number of dredges and various water depths has been carried out and used for an oceanographic study on a regional scale.

2. Regional setting and geochemical approach

2.1. Geological setting

The Mozambique Channel is located in the southwestern Indian Ocean, between the East-African continental margin along Mozambique and Madagascar (Fig. 1A). It resulted from the separation of the eastern part (Madagascar, India, Antarctica and Australia) and the western part of Gondwana (Africa and South America) in the lower Jurassic (McElhinny, 1970; McKenzie, Sclater, 1971). The Antarctic-India-Madagascar structure was relocated southward along a major transform zone called the Davie Fracture Zone (DFZ) to the Upper Cretaceous (Heirtzler and Burroughs, 1971; Coffin and Rabinowitz, 1987; Gaina et al., 2013). This tectonic event is now represented by the Davie Ridge (Fig. 1A), oriented N170, which extends 1200 km east of the African continental margin (15°S) to the Madagascan marginal plateau (22°S). The ridge is punctuated by several seamounts (e.g. Paisley, Macua and Sakalaves) and separates the Comoros basin in the northeast from the deep Mozambique basin in the southwest (Fig. 1A). The major Jurassic structuring phase was followed by the separation of Madagascar and the Antarctic-India block in the Upper Cretaceous, which caused important volcanic activity in Madagascar but also in the Morondava and Majunga basins to the west of the island (Bassias, 1992; Storey et al., 1995; Rogers et al., 2000; Torsvik et al., 2000; Thompson et al., 2019; Fig. 1A). The Eparses Islands (Bassas Da India, Europa, Juan de Nova, and the Glorieuses Islands) have witnessed this volcanic activity since their formation in the Paleocene. Linked to these volcanic events, these islands and the northern part of the Madagascan continental margin are assigned a radiogenic Nd isotope signature of ε_{Nd} ~ 4 (Mahoney et al., 1991; Jeandel et al., 2007), whereas Madagascar presents an Archean signature in the center and in the south, characterized by an average unradiogenic value of ε_{Nd} ~ -25 (from ε_{Nd} = -22 to ε_{Nd} = -28; Paquette et al., 1994; Kröner et al., 2000; Fig. 1B). On the other side of the Mozambique channel, the African continental margin is assigned an

unradiogenic value of ε_{Nd} ~ -20 (Jeandel et al., 2007). This may represents an average of Nd isotope signatures from old continental crustal sources as the Archean Kaapvaal craton (ε_{Nd} ~ -24; Grantham et al., 2011), Zimbabwe craton (ε_{Nd} ~ -29; Jelsma et al., 1996) and Mozambique belt (ε_{Nd} ~ -30; Möller et al., 1998; Fig. 1B) and, younger volcanic sources as the Jurassic Karoo formations with more radiogenic signature of ε_{Nd} ~ -4 (from ε_{Nd} = -9 to ε_{Nd} = 0; Grousset et al., 1992; Jourdan et al., 2007; Fig. 1B).

2.2. Oceanic setting

The Mozambique Channel is a complex oceanic area with (1) exchange between the water masses of the Indian and Atlantic Oceans and (2) the Davie Ridge which constitutes a topographic high ranging from several tens to 100 km in width and characterized by a basement which culminates at 300 meters below sea level (mbsl) and extends to 2500 mbsl (Mougenot et al., 1986; Coffin and Rabinowitz, 1987; Fig. 1C). This ridge separates the Mozambique Channel into distinct basins (Fig. 1A). Warm Indian water masses spread from the Comoros Basin and then are dragged into the Mozambique Current (MC) in the Deep Basin (DiMarco et al., 2002; Quartly et al., 2013; Flemming and Kudrass, 2018). The deep water flows in the Mozambique Undercurrent (MUC) from the south of the Mozambique Basin to the west of the ridge (de Ruijter et al., 2002; Fig. 1B).

The MC is part of the Agulhas Current (AC), which is an essential link for heat and salt exchanges between the Indian and Atlantic Oceans (Gordon, 1986; Weijer, 1999; Lutjerharms, 2006), and is characterized by anticyclonic eddies (ME) up to 300 km in diameter that can affect the entire water column (de Ruijter et al., 2002; Halo et al., 2014; Fig. 1B). The MC transports surface water to a depth of 600 mbsl, composed of Tropical Surface Water (TSW) and Subtropical Surface Water (STSW) but also South Indian Central Water

144 (SICW) between 200 and 600 mbsl (Fig. 1C). The intermediate waters of the MC are
145 composed of Red Sea Water (RSW) between 900 and 1200 mbsl that enters from the north of
146 the Mozambique Channel along the East African coast (Beal et al., 2000; Schott and
147 McCreary, 2001; Fig. 1B, C).
148
149 The MUC and the Agulhas Undercurrent (AUC) carry Antarctic Intermediate Water (AAIW)
150 between 800 and 1500 mbsl (Ullgren et al., 2012; Fig. 1B, C). AAIW arrives from the eastern
151 part of the Mozambique ridge and then flows along the Mozambican coast (Fine, 1993). The
152 North Atlantic Deep Water (NADW) is also part of the MUC, between 1500 and 3500 mbsl
153 (Fig. 1B, C). Its inflow starts upstream of the south of Africa before entering the Mozambique
154 Channel through the Natal Valley (Toole and Warren, 1993). The NADW flows northwards
155 from the Mozambique Basin to the west of the Davie Ridge. Several authors consider that this
156 water mass does not flow over the Davie Ridge and retreats south along the western edge of
157 the ridge (Toole and Warren, 1993, Mantyla and Reid, 1995; You, 2000). Conversely, some
158 authors identified the presence of the NADW beyond the Davie Ridge with circulation along
159 its eastern side after a topographic blockage at 14°S (van Aken et al., 2004; Collins et al.,
160 2016). At a depth of more than 4000 mbsl, the Antarctic Bottom Water (AABW) flows from
161 east of the Mozambique ridge to south of the Mozambique Basin. It is then diverted, before
162 heading south along the Madagascar Ridge (Kolla et al., 1980, Fig. 1B). Finally, north of the
163 Mozambique Channel, the North Indian Deep Water (NIDW) flows at a depth of more than
164 2000 mbsl (Collins et al., 2016; Fig. 1C). It is transported from the Indian Ocean and is
165 present in the northern part of the channel, near the Glorieuses Islands (DiMarco et al., 2002;
166 Fig. 1B). Very few studies have examined the NIDW flow path after its arrival in northern
167 Madagascar and its passage through the Glorieuses Islands. However, new hydrographic data,
168 based on conductivity, temperature, pressure, dissolved oxygen and salinity measurements,

allowed to identify the AAIW, NADW and NIDW water masses beyond the ridge and have proposed new circulation patterns (DiMarco et al., 2002; van Aken, 2004; Collins et al., 2016).

2.3. Geochemical approach

Dissolved Nd in seawater mainly originates from aerosols and continental inputs, through rivers (Goldstein et al., 1984; Goldstein and Jacobsen, 1988; Elderfield et al., 1990; Tachikawa et al., 1997; Ingri et al., 2000; Bayon et al., 2015; van der Lubbe et al., 2016). The Nd isotope composition in seawater can be modified by particulate and dissolved exchange processes along continental margins termed "boundary exchange" (Lacan and Jeandel, 2001, 2005; Rempfer et al., 2011; Pearce et al., 2013. Wilson et al., 2012). In addition, submarine groundwater discharge and benthic fluids from the pore waters of the sediments have been identified as significant sources for Nd in the contributing to REE fluxes to the oceans (Johannesson et al., 2011; Abbott et al., 2015a, 2015b; Haley et al., 2017). However, the relative contribution of these inputs to the overall Nd balance in seawater is still described according to geographic areas (Jones et al., 1994). Ocean Nd residence time is also still debated and supposedly ranges between 600 and 2000 years (Jeandel et al., 1995; Tachikawa et al., 2003; Arsouze et al., 2009; Rempfer et al., 2011), whereas the mixing time of the deep ocean is about 1500 years (Broecker et al., 1982). While being aware of significant changes in local Nd isotope exchange processes or sources, the Nd isotope composition of intermediate and deep waters is therefore expected to be controlled predominantly by conservative mixing between water masses (Goldstein and Hemming, 2003). Nd isotopes are therefore considered as a quasi-conservative tracer of water mass chemistry with potentially great interest in paleoceanographic studies (Frank, 2002; Goldstein and Hemming, 2003). Previous studies of Fe-Mn crusts, nodules and seawater demonstrated that the Atlantic, Indian and Pacific basins each have a distinct and characteristic range in Nd isotope compositions (O'nions et al., 1978; Piepgras et al., 1979). Consequently, Nd isotopes can be used to trace water sourcing and mixing in both the present and past oceans (Piepgras and Wasserburg, 1980, 1982, 1987; Piepgras and Jacobsen, 1988; Jeandel et al., 2013; Amakawa et al., 2019).

The variations of Nd isotope compositions are expressed as:

$$\varepsilon_{\mathrm{Nd}} = \left(\frac{143\mathrm{Nd}/144\mathrm{Nd}\ (\mathrm{meas.})}{143\mathrm{Nd}/144\mathrm{Nd}\ (\mathrm{CHUR})} - 1\right) \times 10^4 \quad (1)$$

where the CHUR (Chondritic Uniform Reservoir) value is 0.512638 (Jacobsen and Wasserburg, 1980). Nd isotope compositions can show significant variations related to erosion and dissolution of rocks in the source regions of water masses. The ε_{Nd} values of the Pacific Ocean range between 0 and -6 resulting from the erosion of very young volcanic rocks derived from the earth mantle mixed with continental inputs that are unradiogenic (Piepgras and Jacobsen, 1988; Shimizu et al., 1994). The water masses of the North Atlantic have ε_{Nd} values between -12 and -14 resulting from erosion of old Canadian shield continental rocks while those of the South Atlantic have ε_{Nd} values between -9 and -11, linked to the mixture between the unradiogenic values of the North Atlantic and the more radiogenic values of the Pacific (Piepgras et al., 1979; Piepgras and Wasserburg, 1982, 1987; Jeandel, 1993). Finally, the Nd isotope composition in the Indian Ocean is a result of the mixture of unradiogenic values of the Atlantic and more radiogenic values of the Pacific Ocean. Its composition ranges between ε_{Nd} = -7 and -8.5 (Bertram and Elderfield, 1993; Arsouze et al., 2007; Wilson et al., 2012). Using Nd isotopes as a tracer of ocean water masses in each ocean basin, it is possible to estimate the respective Atlantic and Pacific contributions to the Indian Ocean by a mixing between the Northwest Atlantic and the Southern Ocean. The equation for conservative Nd isotopic mixing M of the NADW and the Circumpolar Deep Water (CDW) is given by:

$$\varepsilon_{\mathrm{Nd\ (M)}} = \frac{X_{(NADW)}\, C_{(NADW)}\, \varepsilon_{Nd\ (NADW)} + \left(1 - X_{(NADW)}\right) C_{(CDW)}\, \varepsilon_{Nd\ (CDW)}}{X_{(NADW)}\, C_{(NADW)} + \left(1 - X_{(NADW)}\right) C_{(CDW)}} \quad (2)$$

where ε_{Nd} and C are described as the Nd isotope composition and concentration respectively and, X as the mixing proportion. The calculation is based on a Nd isotope composition of ε_{Nd} = -13 and a concentration of 25 pmol/kg for the NADW (Piepgras and Wasserburg, 1982,

219 1987; Jeandel, 1993) and, a Nd isotope composition between ε_{Nd} = -4 and -6 and a
220 concentration of 20 pmol/kg for the CDW (Piepgras and Wasserburg, 1982; Piepgras and
221 Jacobsen, 1988; Jeandel et al., 2013). Thus, for a Nd isotope composition of ε_{Nd} = -7, the
222 Indian water masses can be composed of 15% to 30% of Atlantic water masses and 70% to
223 85% of Pacific water masses with Atlantic ε_{Nd} = -13 and Pacific between ε_{Nd} = -4 and -6,
224 while for a Nd isotope composition of ε_{Nd} = -8.5, the Indian water masses can be composed of
225 25% to 45% of Atlantic water masses and 55% to 75% of Pacific water masses with the same
226 Atlantic and Pacific ε_{Nd}. These calculations are consistent with the method used by Frank et
227 al. (2002) whereby a linear mixing relation between the two Nd end-member water masses is
228 assumed because the Nd concentrations in the NADW and CDW do not present a systematic
229 difference. We applied this approach to calculate NADW contributions to the Mozambique
230 Channel. Table 1 presents a summary of Nd isotope compositions of the main water masses in
231 the Mozambique Channel.

3. Material and methods

3.1. Fe-Mn crust sampling

This work is based on 29 Fe-Mn crust samplings. Locations, depths and other details are given in Table 2 for each sample. 27 were recovered in the Mozambique Channel during the PAMELA-MOZ1 cruise onboard the RV *L'Atalante* (Olu, 2014), as part of the PAMELA (Passive Margin Exploration Laboratory) research project. During this expedition, 22 dredging operations were carried and a total of 186 samples were recovered, including 74 Fe-Mn crusts. 2 other Fe-Mn crusts were recovered during the NOSICAA-MD06 cruise (Agulhas Plateau, sample MNHN-GS-DR75-0012; Leclaire, 1975) and the RIDA-MD39 expedition (western slope of the Davie Ridge, Paisley Mount, sample MNHN-GS-DR84-0026; Leclaire, 1984), conducted by the National Museum of Natural History (MNHN).

Finally, this study is based on 14 sampling stations distributed from the Agulhas Plateau in the south to the Glorieuses Islands north of the Davie Ridge at depths ranging from 580 and 2650 mbsl (Fig. 1A, Table 2), allowing to focus on the geochemical records of all water masses (surface, intermediate and deep).

3.2.Nd isotope measurements

After macroscopic examination, approximately 100 mg of sample were collected from scraping the surface layer of the Fe-Mn crusts. The sampling corresponds to the first 100 µm of the sample, i.e. the last elementary adsorption on Fe and Mn oxyhydroxides, and thus the modern state of water mass geochemistry (Albarède and Goldstein, 1992; Albarède et al., 1997), in the order of 20 to 80 ka due to the slow accretion rates of the studied samples ranging from 1.3 to 5.2 mm/Ma, with an average growth rate of 3.1 mm/Ma in all the samples (Bourlès et al. personal communication). The powders were first dissolved in closed screw-

top Teflon vials (Savillex) at about 100°C for one day using 3 ml of 6 M HCl. The vials where then opened for evaporation at about 130°C. After evaporation to dryness, approximately 2 ml of aqua regia (10 M HCl + 14 M HNO_3) was added, and the vials were capped and put back on the hot plate overnight at about 100°C. The samples were then dried again and taken up in about 6 ml of Quartex 6 M HCl ("mother solutions"). For of Nd isotope compositions analysis, a 2 ml aliquot of the mother solution was dried, and the residue was taken up in about 0.5 ml of Quartex 14.4 M HNO_3 for one hour at 90°C. The vials where then opened for evaporation at about 90°C. After evaporation, 1 ml of 1 M HNO_3 was added and the samples were centrifuged. The REE fraction was separated using Eichrom® Tru spec Resin and the Nd separation was carried out using Eichrom® Ln spec Resin on volumetrically calibrated Teflon columns following an analytical procedure modified from Pin et al. (1994). Nd fractions were loaded on double Re filaments and measured in static mode on a multicollector Thermal Ionization Mass Spectrometer (ThermoScientific Triton) at the "Pôle de Spectrométrie Océan" in Brest, France. The measured $^{143}Nd/^{144}Nd$ ratio was corrected for mass fractionation by normalizing to $^{146}Nd/^{144}Nd = 0.7219$ and the ε_{Nd} values were calculated as expressed in equation (1). Nd isotope composition of standard JNdi was analyzed to monitor instrumental drift. The averaged result of $^{143}Nd/^{144}Nd = 0.512088 \pm 7$ ($2\sigma \times 10^{-6}$; n=14) was consistent with its certified value of $^{143}Nd/^{144}Nd = 0.512115 \pm 7$ ($2\sigma \times 10^{-6}$; Tanaka et al., 2000) corresponding to a LaJolla Nd isotope composition value of $^{143}Nd/^{144}Nd = 0.511858 \pm 7$ ($2\sigma \times 10^{-6}$; Lugmair et al., 1983), so that no instrumental bias had to be taken in account. The standard deviation of this average is ± 0.13 ε_{Nd} unit and associated to each sample analysis. Blank values are below an average of 100 pg and therefore negligible in all cases.

4. Nd isotope compositions

The Nd isotope signatures from the surface layer of the Fe-Mn crusts highlight the large variability (between ε_{Nd} = -7.1 and -10.1) of water mass compositions (Table 2, Fig. 2). In several hydrodynamic and geochemical studies (Toole and Warren, 1993; Jeandel et al., 1995; McCave et al., 2005; Ullgren et al., 2012; Collins et al., 2016), an average water depth of 1500 mbsl is considered to separate intermediate layers (AAIW between 800 and 1500 mbsl, RSW between 900 and 1200 mbsl) from deep layers (NADW and NIDW at more than 1500-2000 mbsl). Therefore, Nd isotope composition of samples located above and below 1500 mbsl will be presented separately (Fig. 3). However, one must note that 4 dredge operations (including 9 samples) were performed both above and just below 1500 mbsl (Fig. 2). For convenience, these results will be included with those obtained on Fe-Mn crusts located strictly above 1500 mbsl; but will be discussed separately.

17 Fe-Mn crusts located above 1500 mbsl were analyzed in this study. South of the Davie Ridge, dredge 19 (DR19) is the shallowest (1000-1350 mbsl). This operation was carried out north of the Jaguar Bank and presents a sample crust with a Nd isotope composition of ε_{Nd} = -7.4 (Table 2, Fig. 3A). The southernmost samples, from dredge 22 (DR22; 1400-1570 mbsl), are located near Europa. For these samples, ε_{Nd} range from -7.8 to -8.7 (n=4). North of these 2 dredges, near Bassas da India, samples collected with dredge 16 (DR16; 1350-1600 mbsl) show unradiogenic compositions of ε_{Nd} = -8.6 and -9.1. In the southern part of the Davie Ridge, south of the Sakalaves Mounts (DR15; 1200-1250 mbsl), the compositions are more radiogenic with ε_{Nd} values of -7.8 and -7.6. At the summit of the Sakalaves Mounts (DR14; 580-650 mbsl), the crust presents an ε_{Nd} = -7.6, whereas north of the Sakalaves Mounts (DR13; 1000-1400 mbsl), the composition is less radiogenic with a value of ε_{Nd} = -8.5. In the northern part of the Davie Ridge, we analyzed 2 Nd isotope compositions on 2 different

crusts. The Fe-Mn crust located on the Macua Mount (DR10; 1000-1400 mbsl) shows radiogenic compositions of ε_{Nd} = -7.8 and -8.0, whereas the sample located on the Paisley Mount on the western slope of the Davie Ridge (DR84-0026; 810 mbsl) exhibits an isotopic composition of ε_{Nd} = -7.1. The analyzed samples from the southwest of Juan de Nova (DR12; 1350-1650 mbsl) show ε_{Nd} values ranging from -7.7 to -7.9 (n=3).

Below 1500 mbsl, 12 Fe-Mn crusts provided Nd isotope compositions. The deepest crust was recovered on the Agulhas Plateau (DR75-0012; 2550 mbsl), 2500 km south of the Davie Ridge (Fig. 1A). It provides an ε_{Nd} value of -10.1 (Table 2, Fig. 3B). Further north, on the east of the Hall Bank (DR17; 1700-1900 mbsl), the ε_{Nd} are -9.0 and -9.4. North of the Davie Ridge, the analyzed samples from the Jeffrey Ridge (DR11; 2400-2450 mbsl) show values ranging between ε_{Nd} = -8.6 and -9.4 (n=4), and the results from the samples located at the Glorieuses Islands (DR01; 2400-2650 mbsl, DR04; 1750-2050 mbsl) attest to more radiogenic Nd isotope compositions in the range of ε_{Nd} = -7.5 to -8.4 (n=5).

5. Discussion

5.1. Characterization of the ε_{Nd} records

5.1.1. Impact of glacial/interglacial variability

Given the relatively slow accretion rates, the 29 studied samples span a time range between 20 and 80 ka, including the record variations of marine isotope stages (MIS) 1 (present to 14 ka), MIS 2 (14 to 29 ka), MIS 3 (29 to 57 ka), MIS 4 (57 to 71 ka) and to a less extent MIS 5 (71 to 130 ka). Changes in the broad patterns of ocean circulation and particles fluxes have been identified between the interglacial MIS 1, 3, 5 and the glacial stages 2, 4 (Curry and Lohmann, 1982; Boyle, 1988; Broecker and Denton, 1990; Rutberg et al., 2000; Bayon et al., 2002; Yu et al., 2008; Roberts et al., 2010; Piotrowski et al., 2004, 2005, 2012; Wei et al., 2016). In particular, Nd isotope variations of Fe-Mn oxide coatings and bulk sediment reductive leachates from southeast Atlantic cores, located near the Cape Basin, indicate cyclical changes with climate stages (Rutberg et al., 2000; Piotrowski et al., 2004, 2005, 2012): during the last glacial maximum (LGM, MIS 2) and the MIS 4 the cores recorded radiogenic ε_{Nd} values ($-6 > \varepsilon_{Nd} > -7$), while the Nd isotope signatures were unradiogenic ($-9 > \varepsilon_{Nd} > -10$) during the interglacial timescales (MIS 1, 3, 5). This variation characterized by a shift of 2 to 3 ε_{Nd} units suggests less NADW flux reached the Southern Ocean during cold stages but an increasing export of NADW during the warm climate intervals (Rutberg et al., 2000), with direct influence on the Nd isotope signature of the Indian deep waters during the MIS (Piotrowski et al.,2009).

However, it has been demonstrated in several studies that, given their slow accumulation rates of few mm/Ma, the Nd isotope records from the outer layers of Fe-Mn oxides represent averages of several glacial/interglacial cycles (Abouchami et al., 1997; Albarède and Goldstein, 1992). The short-term changes in the patterns of ocean circulation and particle

fluxes have had only minor integrated effects (Abouchami et al., 1997; Albarède and Goldstein, 1992). Insofar as the ε_{Nd} measurements of this work are going to be contrasted to present-day seawater Nd isotope signatures, it is important to notice their analysis provides time-integrated information on the ε_{Nd} variations, which can be compared with the modern oceanic circulation (Albarède et al., 1997; Piotrowski et al., 2009; Wilson et al., 2012).

5.1.2. Influence of unradiogenic African margin on ε_{Nd} signatures

As explained in § 2.1, the African continental margin is characterized by an unradiogenic signature of ε_{Nd} ~ -20 (Jeandel et al., 2007), which represents an average of South African Archean cratonic rocks (Jelsma et al., 1996; Möller et al., 1998; De Waele, 2006; Grantham et al., 2011) and younger volcanic sources (Grousset et al., 1992; Jourdan et al., 2007; Fig. 1B). Studies in the modern ocean have suggested that inputs of river loads (van der Lubbe et al., 2016; Rahlf et al., 2020) as well as exchange between particulate and dissolved fractions along African continental margins (Rickli et al., 2010; Stichel et al., 2012b; Wilson et al., 2012) may have an important role on the Nd isotope composition of Atlantic and Indian Oceans. In addition, recent studies have demonstrated that the pore waters can strongly control the REE compositions of the bottom waters (Haley and Klinkhammer, 2003; Schacht et al., 2010; Abbott et al., 2015a, 2015b; Du et al., 2016; Haley et al., 2017; Abbott, 2019).

In the Mozambique Channel, surface waters of the Zambezi and Limpopo discharge have unradiogenic signatures ($-14.7 > \varepsilon_{Nd} > -15.5$ and up to -22.4 respectively; Rahlf et al., 2020). This is thought to influence highly unradiogenic Nd isotope signatures ($\varepsilon_{Nd} = -18.9$ and $\varepsilon_{Nd} = -17.6$) of surface waters (< 600 mbsl) linked to the AC inflow (Stichel et al., 2012b; Rahlf et al., 2020). Moreover, it has been observed that Nd isotope compositions of water masses can be modified up to a spatial variability of ~ 4 ε_{Nd} units due to the boundary exchange process

between seawater and the unradiogenic Madagascan shelf (ε_{Nd} ~ -25; Paquette et al., 1994; Kröner et al., 2000), as shown by Wilson et al. (2012). Our work presents 1 sample from superficial water masses (DR14; 580-650 mbsl) and 6 other Fe-Mn crusts from intermediate waters between 800 and 1400 mbsl (DR10, DR15, DR19 and DR84-0026; Fig. 2). These dredges are spatially spread out over 900 km from the Paisley Mount (DR84-0026) to the Jaguar Bank (DR19) and under the influence of the MC, which spreads from the northern part of the Mozambique Channel and is dragged southbound. 6 of them are located north of the Zambezi (DR84-0026, DR10, DR12, DR13, DR14 and DR15) while the other 3 are situated south of the river mouth (DR16, DR19 and DR22; Fig. 1A).

Considering hypothesis of the Zambezi River loads, the compositions of the samples located in the northern part of the channel are expected to reflect the radiogenic influence of the RSW. Conversely, the crusts located south of the river mouth should indicate unradiogenic Nd isotope signature resulting from Nd continental inputs (Stichel et al., 2012b; Rahlf et al., 2020). In the case of gradual southwards boundary exchange and/or impact of pore waters, it would involve a progressive change of ε_{Nd} signatures. If the MC acquires unradiogenic composition during its spreading along the East African margin as suggested by Wilson et al. (2012), we expect to observe a trend from radiogenic values in the northern part of the channel to unradiogenic signature in the south. However, our results show a narrow range from ε_{Nd} = -7.1 to -8.0 (Fig. 2) and display no abrupt or continuous variations in the Nd isotope signature along the N-S profile. Indeed, the southernmost sample (DR19) presents a value of ε_{Nd} = -7.4 (Table 2, Fig. 3A), whereas it expected to have the more unradiogenic ε_{Nd} whether in the case of river inputs, boundary exchange and/or pore waters influence hypotheses. Moreover, the lowest and the highest ε_{Nd} signatures are observed from DR84-0026 (ε_{Nd} = -7.1) and DR10 (ε_{Nd} = -8.0) located in the northern part of the Mozambique

Channel and distant from 200 km (Fig. 3A). As consequence, our data do not support a major influence of unradiogenic Nd inputs from the river discharges or the continental shelf.

We present 12 samples from the deep water masses (DR01, DR04, DR11, DR17 and DR75-0012; between 1700 and 2550 mbsl; Fig. 2), spatially spread out over 3500 km from the Glorieuses Islands (DR01) to the Agulhas Plateau (DR75-0012; Fig. 3B). In contrast to the crusts from the overlying water masses, these are under the influence of the NADW inflow starting upstream of the south of Africa before entering the Mozambique Channel through the Natal Valley (Toole and Warren, 1993; Fig. 1B). If the unradiogenic Nd isotope addition processes had an impact on the deep water masses, one would predict that this influence would increase as the NADW flows northward. However, the data are increasingly radiogenic towards the north, from ε_{Nd} = -10.2 above the Agulhas Plateau to ε_{Nd} = -7.5 near the Glorieuses Islands (Fig. 3B). Whereas the results of Wilson et al. (2012) present a decreasing radiogenic trend as the boundary exchange occurs, from ε_{Nd} = -8.8 above the Madagascar Ridge to ε_{Nd} = -11.5 in the northeast of the island (Fig. 2). Considering a simple boundary exchange between the African continental margin (ε_{Nd} ~ -20; Jeandel et al., 2007), the NADW arriving from the southern Africa (ε_{Nd} ~ -11; Rahlf et al., 2020) and a boundary exchange rate of 28% calculated by Wilson et al. (2012), the Nd isotope composition of the crust from DR75-0012 is supposed to be ε_{Nd} = -13.5. Furthermore, if the interaction with the unradiogenic margin is continuous from the Agulhas Plateau to the Glorieuses Islands, the results would present Nd isotope compositions considerably lower than ε_{Nd} = -13.5 in all the crusts from the deep waters (DR17, DR11, DR04 and DR01). It would be the same observation in the context of unradiogenic Nd inputs from river discharges or pore waters. However, this is not apparent in our results (ε_{Nd} = -10.2 from the Agulhas Plateau and ε_{Nd} = -

418 7.1 at the Glorieuses Islands; Fig 3B) which are too radiogenic to be explained by the
419 boundary exchange between the NADW and the African shelf.
420
421 Finally, the whole isotopic data of our work are consistent with previous studies (Fig. 2),
422 which are focused on the conservative water mass mixing process in the same geographic area
423 on Fe-Mn crusts (Albarède et al., 1997) and in seawater (Bertram and Elderfield, 1993).
424 Although a slight contribution of the unradiogenic inputs from the African margin cannot be
425 completely ruled out, we assume that our results are mainly due to water mass mixing
426 process. The following sections will therefore discuss of the identification of water masses
427 from Nd isotope compositions and their hydrographic frameworks through the Mozambique
428 Channel.
429

430 ## 5.2. Intermediate layers and Indian water influence (< 1500 mbsl)

431 Above 1500 mbsl, 1 sample provides information on the superficial water masses. Located on
432 the Sakalaves Mounts and at shallow depths (DR14; 580-650 mbsl), this crust displays a
433 value of ε_{Nd} = -7.6 likely corresponding to the Nd isotope composition of the SICW (Fig. 1C,
434 Table 1). This is the only result on this water mass and thus it will not be discussed further
435 here.
436
437 However, the 6 other samples are located between 800 and 1400 mbsl (DR10, DR15, DR19
438 and DR86-0026), illustrating the Nd isotope composition of intermediate water masses. With
439 an range of values between ε_{Nd} = -7.1 and -8.0, these Fe-Mn crusts recorded Indian
440 intermediate water (Tables 1 and 2). This intermediate layer could correspond to the RSW
441 arriving from the north of the Mozambique Channel, following the African continental margin
442 southward (Beal et al., 2000) to the Paisley Mount and the Macua Mount (Fig. 1). The

443 hydrographic flow path of these Indian intermediate water masses south of the Davie Ridge
444 (south of the Sakalaves Mounts and Jaguar Bank) could be explained by the presence of
445 anticyclonic eddies passing through the narrowest part of the Mozambique Channel carrying
446 saline and warm RSW southward as described previously by Ullgren et al. (2012) and
447 Miramontes et al. (2019).
448

449 ## 5.3. Transition zone between intermediate and deep layers

450 The 10 samples from the north of the Sakalaves Mounts (DR13), near Juan de Nova (DR12),
451 Bassas da India and Europa (DR16 and DR22) present ε_{Nd} in the range of -7.7 to -9.1 (Table
452 2, Fig. 2). Both extremes are marked by the influence of distinct water masses. The ε_{Nd} = -9.1
453 (DR16, Bassas da India) is lower and may point out to an Atlantic inflow in the Mozambique
454 Basin. Other values such as ε_{Nd} = -8.7 (DR22, Europa), -8.6 (DR16, Bassas da India) and -8.5
455 (DR13, North of the Sakalava Mounts) also suggest a slight influence of Atlantic currents
456 (Table 1). North of the Davie Ridge, more radiogenic values measured on crusts located near
457 Juan de Nova (ε_{Nd} > -8.0; n=3) correspond to the Indian intermediate water mass inflow as
458 described in § 5.2. However, dredge 22 shows heterogeneous isotopic compositions with one
459 sample at ε_{Nd} = -8.7 that likely indicate Atlantic influence, but also 2 samples with ε_{Nd} > -8.5
460 (-8.2 and -8.1) and one crust with ε_{Nd} > -8.0 (-7.7) suggesting the presence of Indian water
461 mass.
462

463 Therefore, it is imperative to understand why both Atlantic and Indian water mass inflows are
464 recorded in the same area (Fig. 3A). Two assumptions can be considered. The first is the
465 confrontation of the AAIW and RSW intermediate currents whose depths and thicknesses are
466 relatively similar (Fig, 1C, Table 1). In this case, the Nd isotope variations observed would be
467 related to mixing of the unradiogenic AAIW that enters from the south of the channel, and the

more radiogenic RSW arriving from the northwest part of the Mozambique Channel (Fig. 1C). The unradiogenic results would be related to a strong AAIW influence whereas the more radiogenic values would correspond to a robust RSW inflow in the channel. However, the integrated time in these surface scraping is in the order of 30 to 80 ka due to the slow accretion rates of this studied samples ranging from 1.3 to 3.6 mm/Ma. It provides time-integrated information on the sources of Nd (Albarède et al., 1997; Frank et al., 2002) and, should streamline water mass variations mainly related to glacial and interglacial changes. In this case, the recorded isotopic compositions should be relatively homogeneous. The second hypothesis heeds the depths of the starting and ending points of dredge operations (e.g. DR16; 1600-1350 mbsl), which can lead to the recovery of Fe-Mn crusts that are under the influence of deep water masses (NADW, NIDW) and/or intermediate water masses (RSW, AAIW; Table 1, Fig. 2). Thus, within the same dredge (i.e. DR22; 1400-1550 mbsl), some samples could have recorded the isotopic composition of the intermediate currents while others could have recorded the isotopic signature of a transition zone between intermediate and deep water masses (Fig. 2). In this case, differences in the recorded Nd isotope compositions would be related to the thickness variations of the water masses in the Mozambique Channel over the last 100 ka.

5.4. Deep layers (> 1500 mbsl)

The Nd isotope compositions, recorded on Fe-Mn crusts located between 1700 and 2650 mbsl, provided a significant number of results (n=12) with a clear isotopic trend from the south to the north of the Mozambique Channel (Fig. 3BB). Southwestern of the Davie Ridge, the crust from the Agulhas Plateau (DR75-0012) presents an unradiogenic result of ε_{Nd} = -10.1 likely reflecting Atlantic deep water arrival in the Mozambique Channel (Fig. 1B, Table 1). Using the calculation of Frank et al. (2002), the contribution of the NADW is estimated at

493 60% in the Agulhas Plateau fixing Atlantic seawater ε_{Nd} = -13 and Pacific seawater ε_{Nd} = -6
494 (68% with Pacific seawater ε_{Nd} = -4; Table 2, Fig. 4). This percentage is supported by the
495 study of Rahlf et al. (2020), which estimates a mixing between a NADW fraction of up to 80-
496 90% with the CDW eastern Cape Basin. The contribution of NADW then decreases
497 southward, reflecting a gradual dilution with southern waters. Its influence is recorded all the
498 way to the Hall Bank with values ε_{Nd} = -9.0 and -9.4 (DR17). In this area the NADW inflow is
499 calculated between 43% and 48% (56% and 60% with Pacific seawater ε_{Nd} = -4; Table 2, Fig.
500 4). By contrast, in the north of the Mozambique Channel, near the Glorieuses Islands (DR01
501 and DR04), the Nd isotope compositions are more radiogenic (-7.5 > ε_{Nd} > -8.4; n=5)
502 corresponding to the Indian Ocean influence by the arrival of the NIDW in the Comoros
503 Basin (Fig. 1B, Table 1). In the northern part of the channel, the contribution of the NADW is
504 estimated between 21% and 34% (39% and 49% with Pacific seawater ε_{Nd} = -4; Table 2, Fig.
505 4). These values correspond to the contributions of Atlantic water masses in the mixing with
506 Pacific water masses in the current Indian Ocean. Therefore, the NADW from the south of the
507 Mozambique Channel does not seem to be present in the northern part of the Comoros Basin.
508 However, less radiogenic compositions (up to ε_{Nd} = -9.4; DR11) were recorded north of the
509 Davie Ridge, on a ridge in the Comoros Basin, 90 km north of Juan de Nova and 700 km
510 southwest of the Glorieuses Islands (Table 2, Fig. 3B). These unradiogenic values cannot be
511 explained solely by the presence of the NIDW in the northern part of the Mozambique
512 Channel. The inflow of the NADW is estimated between 37% and 48% (51% and 60% with
513 Pacific seawater ε_{Nd} = -4; Table 2, Fig. 4). These estimates of the Atlantic inflow show that a
514 significant portion of the NADW crosses the Davie Ridge and flows into the northern part of
515 the channel without reaching the Glorieuses Islands.
516

517 ## 5.5. NADW northern boundary

518 This study reveals a trend based on Nd isotope compositions of Fe-Mn crusts from
519 unradiogenic values in the south of the Africa, on the Agulhas Plateau, to more radiogenic
520 values in the north of the Mozambique Channel (Table 2, Fig. 3). For the first time it is
521 possible to identify and quantify the NADW influence in the Mozambique Channel to the
522 Comoros Basin through a geochemical study of Fe-Mn crusts (Fig. 4). The only research
523 carried out on Fe-Mn crusts in this area is that of Albarède et al. (1997, Fig. 2), indicating
524 unradiogenic value in the southwestern part of the Mozambique Channel as presented before
525 but an isocontour of ε_{Nd} = -8 upstream of the Mozambique Basin and Madagascar. This
526 isotope limit suggests a significant restriction of the NADW input into the Mozambique
527 Channel which is not consistent with our results, suggesting this isotope limit further north
528 and most importantly north of the Davie Ridge (Fig. 4). The differences in the Nd isotope
529 values between both studies are undoubtedly related to the depth of the samples. Indeed,
530 Albarède et al. (1997) were interested in Nd global trends in the oceans. In the centre part of
531 the Mozambique Channel, their isotopic analyses were measured on crusts from surface
532 layers (~ 600 mbsl; Fig. 2). As described in previous sections, these water masses have Nd
533 isotope signatures from the Indian Ocean (Table 1) and are therefore naturally much more
534 radiogenic than the results of our study, which also focuses on intermediate and deep water
535 mass flow path.
536
537 Simultaneously, two major hydrographic studies advance scientific knowledge on the Atlantic
538 and Indian deep currents in the Mozambique Channel. Van Aken et al. (2004) noted the
539 influence of the NADW current at depths between 1500 and 2500 mbsl in the channel. This
540 was supported and expanded upon by the hydrographic research of Collins et al. (2016). The
541 NADW and NIDW currents were recorded in the Comoros Basin, according to their salinity
542 and oxygen levels. The current flow path of these deep water masses in the Mozambique

Channel is therefore a visible and currently quantified phenomenon. Our study confirms the presence of the NADW in the northern part of the channel and strongly suggests a passage of the NADW beyond the Davie Ridge (Fig. 4), implying that this topographic barrier does not currently act as an impassable obstacle to the circulation of deep currents in the Mozambique Channel.

6. Summary and conclusion

Fe-Mn crusts are highly studied ocean resources in terms of their geochemical composition as archives of the chemical composition of water masses. The analysis of 29 crusts sampled in the Mozambique Channel show Nd isotope records ranging from unradiogenic values (ε_{Nd} = -10.1) in the Agulhas Plateau to more radiogenic values (ε_{Nd} = -7.5) north of the Mozambique Channel, near the Glorieuses Islands.

First, this study reveals the presence of the Indian intermediate seawater above 1500 mbsl. Secondly, the crusts dredged at depths between 1300 and 1650 mbsl show significant isotopic variations (between ε_{Nd} = -7.7 and -9.1), probably due to their location in a transition zone between intermediate and deep water masses with contrasted Nd isotope signatures. Finally, unradiogenic compositions are recorded beyond the Davie Ridge. These new results suggest significant contributions of the NADW flowing from the south below 1500 mbsl and crossing the Davie Ridge to be recorded in the northern part of the Mozambique Channel, in the Comoros Basin.

This unique collection of crust samples improves our understanding of the Atlantic and Indian water mass flow path in this complex area. As this key area of oceanic mixing has undergone diverse geodynamic movements, it would be interesting to carry out isotope studies on several time series distributed from the Agulhas Plateau to the Glorieuses Islands at different depths (especially in the transition zone). These future studies would allow to identify and understand major geodynamic and oceanographic events in the Mozambique Channel up to the Miocene.

Acknowledgments

We thank the Captains, crews and onboard scientific teams of the PAMELA-MOZ01 survey onboard the R/V *L'Atalante* and, the RIDA-MD39 and the NOSICAA-MD06 surveys onboard the R/V Marion Dufresne. The oceanographic survey PAMELA-MOZ01, as well as Claire CHARLES PhD are co-funded by TOTAL and IFREMER as part of the PAMELA (Passive Margin Exploration Laboratories) scientific project. The PAMELA project is a scientific project led by Ifremer and TOTAL in collaboration with the Université de Bretagne Occidentale, Université Rennes 1, Université Pierre et Marie Curie, CNRS and IFPEN. The authors are grateful to Anne-Sophie Alix, Philippe Fernagu and Thierry Dalle Mulle for their help and the crust-sample preparation. We also thank the MNHN, Eva Moreno and Lola Johannes for allowing us to access and borrow samples from the RIDA-MD39 and NOSICAA-MD06 oceanographic expeditions belonging to the oceanic collection. We gratefully acknowledge Editor-in-Chief Michele Rebesco, Guest Editor Vittorio Maselli, Jean-Carlos Montero-Serrano and an anonymous reviewer for thorough and thoughtful comments that significantly improved the manuscript.

References

Abbott, A.N., 2019. A benthic flux from calcareous sediments results in non-conservative neodymium behavior during lateral transport: A study from the Tasman Sea. Geology 47, 363–366. https://doi.org/10.1130/G45904.1

Abbott, A.N., Haley, B.A., McManus, J., 2015a. Bottoms up: Sedimentary control of the deep North Pacific Ocean's εNd signature. Geology 43, 1035–1035. https://doi.org/10.1130/G37114.1

Abbott, A.N., Haley, B.A., McManus, J., Reimers, C.E., 2015b. The sedimentary flux of dissolved rare earth elements to the ocean. Geochim. Cosmochim. Acta 154, 186–200. https://doi.org/10.1016/j.gca.2015.01.010

Abouchami, W., Goldstein, S.L., Gazer, S.J.G., Eisenhauer, A., Mangini, A., 1997. Secular changes of lead and neodymium in central Pacific seawater recorded by a Fe·Mn crust. Geochim. Cosmochim. Acta 61, 3957–3974. https://doi.org/10.1016/S0016-7037(97)00218-4

Albarède, F., Goldstein, S.L., 1992. World map of Nd isotopes in sea-floor ferromanganese deposits. Geology 20, 761–763. https://doi.org/10.1130/0091-7613(1992)020<0761:WMONII>2.3.CO;2

Albarède, F., Goldstein, S.L., Dautel, D., 1997. The neodymium isotopic composition of manganese nodules from the Southern and Indian oceans, the global oceanic neodymium budget, and their bearing on deep ocean circulation. Geochim. Cosmochim. Acta 61, 1277–1291. https://doi.org/10.1016/S0016-7037(96)00404-8

611 Albarède, F., Simonetti, A., Vervoort, J.D., Blichert-Toft, J., Abouchami, W., 1998. A Hf-Nd
612 isotopic correlation in ferromanganese nodules. Geophys. Res. Lett. 25, 3895–3898.
613 https://doi.org/10.1029/1998GL900008
614
615 Amakawa, H., Tazoe, H., Obata, H., Gamo, T., Sano, Y., Shen, C.-C., 2013. Neodymium
616 isotopic composition and concentration in the Southwest Pacific Ocean. Geochem. J. 47, 409–
617 422. https://doi.org/10.2343/geochemj.2.0260
618
619 Amakawa, H., Yu, T.-L., Tazoe, H., Obata, H., Gamo, T., Sano, Y., Shen, C.-C., Suzuki, K.,
620 2019. Neodymium concentration and isotopic composition distributions in the southwestern
621 Indian Ocean and the Indian sector of the Southern Ocean. Chem. Geol. 511, 190–203.
622 https://doi.org/10.1016/j.chemgeo.2019.01.007
623 Aplin, A., Cronan, D., 1985. Ferromanganese oxide deposits from the Central Pacific Ocean,
624 I. Encrustations from the Line Islands Archipelago. Geochim. Cosmochim. Acta 49, 427–436.
625 https://doi.org/10.1016/0016-7037(85)90034-1
626
627 Aplin, A., Michard, A., Albarède, F., 1986. 143Nd/144Nd in Pacific ferromanganese
628 encrustations and nodules. Earth Planet. Sci. Lett. 81, 7–14. https://doi.org/10.1016/0012-
629 821X(86)90096-8
630
631 Arsouze, T., Dutay, J.-C., Lacan, F., Jeandel, C., 2009. Reconstructing the Nd oceanic cycle
632 using a coupled dynamical – biogeochemical model. Biogeosciences 6, 2829–2846.
633 https://doi.org/10.5194/bg-6-2829-2009
634

635 Arsouze, T., Dutay, J.-C., Lacan, F., Jeandel, C., 2007. Modeling the neodymium isotopic
636 composition with a global ocean circulation model. Chem. Geol. 239, 165–177.
637 https://doi.org/10.1016/j.chemgeo.2006.12.006
638
639 Bassias, Y., 1992. Petrological and geochemical investigation of rocks from the Davie
640 fracture zone (Mozambique Channel) and some tectonic implications. J. Afr. Earth Sci.
641 Middle East 15, 321–339. https://doi.org/10.1016/0899-5362(92)90018-8
642
643 Bayon, G., German, C.R., Boella, R.M., Milton, J.A., Taylor, R.N., Nesbitt, R.W., 2002. An
644 improved method for extracting marine sediment fractions and its application to Sr and Nd
645 isotopic analysis. Chem. Geol. 187, 179–199. https://doi.org/10.1016/S0009-2541(01)00416-
646 8
647
648 Bayon, G., Toucanne, S., Skonieczny, C., André, L., Bermell, S., Cheron, S., Dennielou, B.,
649 Etoubleau, J., Freslon, N., Gauchery, T., Germain, Y., Jorry, S.J., Ménot, G., Monin, L.,
650 Ponzevera, E., Rouget, M.-L., Tachikawa, K., Barrat, J.A., 2015. Rare earth elements and
651 neodymium isotopes in world river sediments revisited. Geochim. Cosmochim. Acta 170, 17–
652 38. https://doi.org/10.1016/j.gca.2015.08.001
653
654 Beal, L.M., Ffield, A., Gordon, A.L., 2000. Spreading of Red Sea overflow waters in the
655 Indian Ocean. J. Geophys. Res. Oceans 105, 8549–8564.
656 https://doi.org/10.1029/1999JC900306
657

Bertram, C.J., Elderfield, H., 1993. The geochemical balance of the rare earth elements and neodymium isotopes in the oceans. Geochim. Cosmochim. Acta 57, 1957–1986. https://doi.org/10.1016/0016-7037(93)90087-D

Bourlès, D., Raisbeck, G.M., Yiou, F., 1989. 10Be and 9Be in marine sediments and their potential for dating. Geochim. Cosmochim. Acta 53, 443–452. https://doi.org/10.1016/0016-7037(89)90395-5

Boyle, E.A., 1988. Vertical oceanic nutrient fractionation and glacial/interglacial CO2 cycles. Nature 331, 55–56. https://doi.org/10.1038/331055a0

Broecker, W.S., Denton, G.H., 1990. The role of ocean-atmosphere reorganizations in glacial cycles. Quat. Sci. Rev. 9, 305–341. https://doi.org/10.1016/0277-3791(90)90026-7

Broecker, W.S., Peng, T., Beng, Z., 1982. Tracers in the sea. Lamont-Doherty Geological Observatory, Columbia University.

Christensen, J.N., Halliday, A.N., Godfrey, L.V., Hein, J.R., Rea, D.K., 1997. Climate and Ocean Dynamics and the Lead Isotopic Records in Pacific Ferromanganese Crusts. Science 277, 913–918. https://doi.org/10.1126/science.277.5328.913

Coffin, M.F., Rabinowitz, P.D., 1987. Reconstruction of Madagascar and deep: Evidence from the Davie Fracture Zone and Western Somali Basin. J. Geophys. Res. Solid Earth 92, 9385–9406. https://doi.org/10.1029/JB092iB09p09385

683 Collins, C., Hermes, J.C., Roman, R.E., Reason, C.J.C., 2016. First dedicated hydrographic
684 survey of the Comoros Basin. J. Geophys. Res. Oceans 121, 1291–1305.
685 https://doi.org/10.1002/2015JC011418
686
687 Curry, W.B., Lohmann, G.P., 1982. Carbon Isotopic Changes in Benthic Foraminifera from
688 the Western South Atlantic: Reconstruction of Glacial Abyssal Circulation Patterns. Quat.
689 Res. 18, 218–235. https://doi.org/10.1016/0033-5894(82)90071-0
690
691 de Ruijter, W.P.M., Ridderinkhof, H., Lutjeharms, J.R.E., Schouten, M.W., Veth, C., 2002.
692 Observations of the flow in the Mozambique Channel: OBSERVATIONS IN THE
693 MOZAMBIQUE CHANNEL. Geophys. Res. Lett. 29, 140-1-140–3.
694 https://doi.org/10.1029/2001GL013714
695
696 De Waele, B., Liégeois, J.-P., Nemchin, A.A., Tembo, F., 2006. Isotopic and geochemical
697 evidence of proterozoic episodic crustal reworking within the irumide belt of south-central
698 Africa, the southern metacratonic boundary of an Archaean Bangweulu Craton. Precambrian
699 Res. 148, 225–256. https://doi.org/10.1016/j.precamres.2006.05.006
700
701 DiMarco, S.F., Chapman, P., Nowlin, W.D., Hacker, P., Donohue, K., Luther, M., Johnson,
702 G.C., Toole, J., 2002. Volume transport and property distributions of the Mozambique
703 Channel. Deep Sea Res. Part II Top. Stud. Oceanogr. 49, 1481–1511.
704 https://doi.org/10.1016/S0967-0645(01)00159-X
705
706 Du, J., Haley, B.A., Mix, A.C., 2016. Neodymium isotopes in authigenic phases, bottom
707 waters and detrital sediments in the Gulf of Alaska and their implications for paleo-circulation

reconstruction. Geochim. Cosmochim. Acta 193, 14–35. https://doi.org/10.1016/j.gca.2016.08.005

Eisenhauer, A., Gögen, K., Pernicka, E., Mangini, A., 1992. Climatic influences on the growth rates of Mn crusts during the Late Quaternary. Earth Planet. Sci. Lett. 109, 25–36. https://doi.org/10.1016/0012-821X(92)90071-3

Elderfield, H., Upstill-Goddard, R., Sholkovitz, E.R., 1990. The rare earth elements in rivers, estuaries, and coastal seas and their significance to the composition of ocean waters. Geochim. Cosmochim. Acta 54, 971–991. https://doi.org/10.1016/0016-7037(90)90432-K

Fine, R.A., 1993. Circulation of Antarctic intermediate water in the South Indian Ocean. Deep Sea Res. Part Oceanogr. Res. Pap. 40, 2021–2042. https://doi.org/10.1016/0967-0637(93)90043-3

Flemming, B.W., Kudrass, H.-R., 2018. Large dunes on the outer shelf off the Zambezi Delta, Mozambique: evidence for the existence of a Mozambique Current. Geo-Mar. Lett. 38, 95–106. https://doi.org/10.1007/s00367-017-0515-5

Frank, M., 2002. Radiogenic isotopes: tracers of past ocean circulation and erosional input. Rev. Geophys. 40, 1–1. https://doi.org/10.1029/2000RG000094

Frank, M., O'Nions, R.K., 1998. Sources of Pb for Indian Ocean ferromanganese crusts: a record of Himalayan erosion? Earth Planet. Sci. Lett. 158, 121–130. https://doi.org/10.1016/S0012-821X(98)00055-7

733

734 Frank, M., O'Nions, R.K., Hein, J.R., Banakar, V.K., 1999. 60 Myr records of major elements
735 and Pb–Nd isotopes from hydrogenous ferromanganese crusts: reconstruction of seawater
736 paleochemistry. Geochim. Cosmochim. Acta 63, 1689–1708. https://doi.org/10.1016/S0016-
737 7037(99)00079-4

738

739 Frank, M., Whiteley, N., Kasten, S., Hein, J.R., O'Nions, K., 2002. North Atlantic Deep
740 Water export to the Southern Ocean over the past 14 Myr: Evidence from Nd and Pb isotopes
741 in ferromanganese crusts. Paleoceanography 17, 12-1-12–9.
742 https://doi.org/10.1029/2000PA000606

743

744 Gaina, C., Torsvik, T.H., van Hinsbergen, D.J.J., Medvedev, S., Werner, S.C., Labails, C.,
745 2013. The African Plate: A history of oceanic crust accretion and subduction since the
746 Jurassic. Tectonophysics, Progress in understanding the South Atlantic margins 604, 4–25.
747 https://doi.org/10.1016/j.tecto.2013.05.037

748

749 Goldstein, S.L., Hemming, S.R., 2003. 6.17 - Long-lived Isotopic Tracers in Oceanography,
750 Paleoceanography, and Ice-sheet Dynamics, in: Holland, H.D., Turekian, K.K. (Eds.),
751 Treatise on Geochemistry. Pergamon, Oxford, pp. 453–489. https://doi.org/10.1016/B0-08-
752 043751-6/06179-X

753

754 Goldstein, S.J., Jacobsen, S.B., 1988. Rare earth elements in river waters. Earth Planet. Sci.
755 Lett. 89, 35–47. https://doi.org/10.1016/0012-821X(88)90031-3

756

757 Goldstein, S.L., O'Nions, R.K., Hamilton, P.J., 1984. A Sm-Nd isotopic study of atmospheric
758 dusts and particulates from major river systems. Earth Planet. Sci. Lett. 70, 221–236.
759 https://doi.org/10.1016/0012-821X(84)90007-4
760
761 Gordon, A.L., 1986. Interocean exchange of thermocline water. J. Geophys. Res. Oceans 91,
762 5037–5046. https://doi.org/10.1029/JC091iC04p05037
763
764 Grantham, G.H., Manhica, A.D.S.T., Armstrong, R.A., Kruger, F.J., Loubser, M., 2011. New
765 SHRIMP, Rb/Sr and Sm/Nd isotope and whole rock chemical data from central Mozambique
766 and western Dronning Maud Land, Antarctica: Implications for the nature of the eastern
767 margin of the Kalahari Craton and the amalgamation of Gondwana. J. Afr. Earth Sci. 59, 74–
768 100. https://doi.org/10.1016/j.jafrearsci.2010.08.005
769
770 Grousset, F.E., Biscaye, P.E., Revel, M., Petit, J.-R., Pye, K., Joussaume, S., Jouzel, J., 1992.
771 Antarctic (Dome C) ice-core dust at 18 k.y. B.P.: Isotopic constraints on origins. Earth Planet.
772 Sci. Lett. 111, 175–182. https://doi.org/10.1016/0012-821X(92)90177-W
773
774 Haley, B.A., Du, J., Abbott, A.N., McManus, J., 2017. The Impact of Benthic Processes on
775 Rare Earth Element and Neodymium Isotope Distributions in the Oceans. Front. Mar. Sci. 4.
776 https://doi.org/10.3389/fmars.2017.00426
777
778 Haley, B.A., Klinkhammer, G.P., 2003. Complete separation of rare earth elements from
779 small volume seawater samples by automated ion chromatography: method development and
780 application to benthic flux. Mar. Chem. 82, 197–220. https://doi.org/10.1016/S0304-
781 4203(03)00070-7

Halo, I., Backeberg, B., Penven, P., Ansorge, I., Reason, C., Ullgren, J.E., 2014. Eddy properties in the Mozambique Channel: A comparison between observations and two numerical ocean circulation models. Deep Sea Res. Part II Top. Stud. Oceanogr. 100, 38–53. https://doi.org/10.1016/j.dsr2.2013.10.015

Hein, J.R., Conrad, T.A., Dunham, R.E., 2009. Seamount Characteristics and Mine-Site Model Applied to Exploration- and Mining-Lease-Block Selection for Cobalt-Rich Ferromanganese Crusts. Mar. Georesources Geotechnol. 27, 160–176. https://doi.org/10.1080/10641190902852485

Hein, J.R., Conrad, T.A, Mizell, K., Banakar, V.K., Frey, F.A., Sager, W.W., 2016. Controls on ferromanganese crust composition and reconnaissance resource potential, Ninetyeast Ridge, Indian Ocean.

Hein, J.R., Conrad, T.A., Staudigel, H., 2010. Seamount Mineral Deposits: a source of rare metals for high-technology industries. Oceanography 23, 184–189.

Hein, J.R., Koschinsky, A., Halbach, P., Manheim, F.T., Bau, M., Kang, J.-K., Lubick, N., 1997. Iron and manganese oxide mineralization in the Pacific. Geol. Soc. Lond. Spec. Publ. 119, 123–138. https://doi.org/10.1144/GSL.SP.1997.119.01.09

Heirtzler, J.R., Burroughs, R.H., 1971. Madagascar's Paleoposition: New Data from the Mozambique Channel. Science 174, 488–490. https://doi.org/10.1126/science.174.4008.488

807 Ingri, J., Widerlund, A., Land, M., Gustafsson, Ö., Andersson, P., Öhlander, B., 2000.
808 Temporal variations in the fractionation of the rare earth elements in a boreal river; the role of
809 colloidal particles. Chem. Geol. 166, 23–45. https://doi.org/10.1016/S0009-2541(99)00178-3
810
811 Jacobsen, S.B., Wasserburg, G.J., 1980. Sm-Nd isotopic evolution of chondrites. Earth Planet.
812 Sci. Lett. 50, 139–155. https://doi.org/10.1016/0012-821X(80)90125-9
813
814 Jeandel, C., 1993. Concentration and isotopic composition of Nd in the South Atlantic Ocean.
815 Earth Planet. Sci. Lett. 117, 581–591. https://doi.org/10.1016/0012-821X(93)90104-H
816
817 Jeandel, C., Arsouze, T., Lacan, F., Téchiné, P., Dutay, J.-C., 2007. Isotopic Nd compositions
818 and concentrations of the lithogenic inputs into the ocean: A compilation, with an emphasis
819 on the margins. Chem. Geol. 239, 156–164. https://doi.org/10.1016/j.chemgeo.2006.11.013
820
821 Jeandel, C., Bishop, J.K., Zindler, A., 1995. Exchange of neodymium and its isotopes
822 between seawater and small and large particles in the Sargasso Sea. Geochim. Cosmochim.
823 Acta 59, 535–547. https://doi.org/10.1016/0016-7037(94)00367-U
824
825 Jeandel, C., Delattre, H., Grenier, M., Pradoux, C., Lacan, F., 2013. Rare earth element
826 concentrations and Nd isotopes in the Southeast Pacific Ocean. Geochem. Geophys.
827 Geosystems 14, 328–341. https://doi.org/10.1029/2012GC004309
828
829 Jelsma, H.A., Vinyu, M.L., Wijbrans, J.R., Verdurmen, E.A.T., Valbracht, P.J., Davies, G.R.,
830 Valbracht, P.J., 1996. Constraints on Archaean crustal evolution of the Zimbabwe craton: a

U-Pb zircon, Sm-Nd and Pb-Pb whole-rock isotope study. Contrib. Mineral. Petrol. 124, 55–70. https://doi.org/10.1007/s004100050173

Johannesson, K.H., Chevis, D.A., Burdige, D.J., Cable, J.E., Martin, J.B., Roy, M., 2011. Submarine groundwater discharge is an important net source of light and middle REEs to coastal waters of the Indian River Lagoon, Florida, USA. Geochim. Cosmochim. Acta 75, 825–843. https://doi.org/10.1016/j.gca.2010.11.005

Jones, C.E., Halliday, A.N., Rea, D.K., Owen, R.M., 1994. Neodymium isotopic variations in North Pacific modern silicate sediment and the insignificance of detrital REE contributions to seawater. Earth Planet. Sci. Lett. 127, 55–66. https://doi.org/10.1016/0012-821X(94)90197-X

Jourdan, F., Bertrand, H., Schärer, U., Blichert-Toft, J., Féraud, G., Kampunzu, A.B., 2007. Major and Trace Element and Sr, Nd, Hf, and Pb Isotope Compositions of the Karoo Large Igneous Province, Botswana–Zimbabwe: Lithosphere vs Mantle Plume Contribution. J. Petrol. 48, 1043–1077. https://doi.org/10.1093/petrology/egm010

Kolla, V., Eittreim, S., Sullivan, L., Kostecki, J.A., Burckle, L.H., 1980. Current-controlled, abyssal microtopography and sedimentation in Mozambique Basin, southwest Indian Ocean. Mar. Geol. 34, 171–206. https://doi.org/10.1016/0025-3227(80)90071-7

Koschinsky, A., Halbach, P., 1995. Sequential leaching of marine ferromanganese precipitates: Genetic implications. Geochim. Cosmochim. Acta 59, 5113–5132. https://doi.org/10.1016/0016-7037(95)00358-4

856 Koschinsky, A., Stascheit, A., Bau, M., Halbach, P., 1997. Effects of phosphatization on the
857 geochemical and mineralogical composition of marine ferromanganese crusts. Geochim.
858 Cosmochim. Acta 61, 4079–4094. https://doi.org/10.1016/S0016-7037(97)00231-7
859
860 Kröner, A., Hegner, E., Collins, A.S., Windley, B.F., Brewer, T.S., Razakamanana, T.,
861 Pidgeon, R.T., 2000. Age and magmatic history of the Antananarivo Block, central
862 Madagascar, as derived from zircon geochronology and Nd isotopic systematics. Am. J. Sci.
863 300, 251–288. https://doi.org/10.2475/ajs.300.4.251
864
865 Kusakabe, M., Ku, T.-L., 1984. Incorporation of Be isotopes and other trace metals into
866 marine ferromanganese deposits. Geochim. Cosmochim. Acta 48, 2187–2193.
867 https://doi.org/10.1016/0016-7037(84)90215-1
868
869 Lacan, F., Jeandel, C., 2005. Neodymium isotopes as a new tool for quantifying exchange
870 fluxes at the continent–ocean interface. Earth Planet. Sci. Lett. 232, 245–257.
871 https://doi.org/10.1016/j.epsl.2005.01.004
872
873 Lacan, F., Jeandel, C., 2001. Tracing Papua New Guinea imprint on the central Equatorial
874 Pacific Ocean using neodymium isotopic compositions and Rare Earth Element patterns.
875 Earth Planet. Sci. Lett. 186, 497–512. https://doi.org/10.1016/S0012-821X(01)00263-1
876
877 Leclaire, L., 1984. RIDA-MD39, RV Marion Dufresne. https://doi.org/10.17600/84010511
878
879 Leclaire, L., 1975. NOSICAA-MD06, RV Marion Dufresne.
880 https://doi.org/10.17600/75010711

881

882 Ling, H.F., Burton, K.W., O'Nions, R.K., Kamber, B.S., von Blanckenburg, F., Gibb, A.J.,
883 Hein, J.R., 1997. Evolution of Nd and Pb isotopes in Central Pacific seawater from
884 ferromanganese crusts. Earth Planet. Sci. Lett. 146, 1–12. https://doi.org/10.1016/S0012-
885 821X(96)00224-5

886

887 Lugmair, G.W., Shimamura, T., Lewis, R.S., Anders, E., 1983. Samarium-146 in the Early
888 Solar System: Evidence from Neodymium in the Allende Meteorite. Science 222, 1015–1018.
889 https://doi.org/10.1126/science.222.4627.1015

890

891 Lusty, P.A.J., Hein, J.R., Josso, P., 2018. Formation and Occurrence of Ferromanganese
892 Crusts: Earth's Storehouse for Critical Metals. Elements 14, 313–318.
893 https://doi.org/10.2138/gselements.14.5.313

894

895 Lutjeharms, J.R.E., 2006. The Agulhas Current. Springer-Verlag, Berlin Heidelberg.

896

897 Mahoney, J., Nicollet, C., Dupuy, C., 1991. Madagascar basalts: tracking oceanic and
898 continental sources. Earth Planet. Sci. Lett. 104, 350–363. https://doi.org/10.1016/0012-
899 821X(91)90215-4

900

901 Manheim, F.T., Lane-Bostwick, C.M., 1988. Cobalt in ferromanganese crusts as a monitor of
902 hydrothermal discharge on the Pacific sea floor. Nature 335, 59.
903 https://doi.org/10.1038/335059a0

904

905 Mantyla, A.W., Reid, J.L., 1995. On the origins of deep and bottom waters of the Indian
906 Ocean. J. Geophys. Res. Oceans 100, 2417–2439. https://doi.org/10.1029/94JC02564
907
908 McCave, I.N., Kiefer, T., Thornalley, D.J.R., Elderfield, H., 2005. Deep flow in the
909 Madagascar Mascarene Basin over the last 150000 years. Philos. Trans. R. Soc. Math. Phys.
910 Eng. Sci.
911
912 McElhinny, M.W., 1970. Formation of the Indian Ocean. Nature 228, 977.
913 https://doi.org/10.1038/228977a0
914
915 McKenzie, D., Sclater, J.G., 1971. The Evolution of the Indian Ocean since the Late
916 Cretaceous. Geophys. J. Int. 24, 437–528. https://doi.org/10.1111/j.1365-
917 246X.1971.tb02190.x
918
919 Miramontes, E., Penven, P., Fierens, R., Droz, L., Toucanne, S., Jorry, S.J., Jouet, G., Pastor,
920 L., Silva Jacinto, R., Gaillot, A., Giraudeau, J., Raisson, F., 2019. The influence of bottom
921 currents on the Zambezi Valley morphology (Mozambique Channel, SW Indian Ocean): In
922 situ current observations and hydrodynamic modelling. Mar. Geol. 410, 42–55.
923 https://doi.org/10.1016/j.margeo.2019.01.002
924
925 Möller, A., Mezger, K., Schenk, V., 1998. Crustal Age Domains and the Evolution of the
926 Continental Crust in the Mozambique Belt of Tanzania: Combined Sm–Nd, Rb–Sr, and Pb–
927 Pb Isotopic Evidence. J. Petrol. 39, 749–783. https://doi.org/10.1093/petroj/39.4.749
928

929 Mougenot, D., Recq, M., Virlogeux, P., Lepvrier, C., 1986. Seaward extension of the East
930 African Rift. Nature 321, 599. https://doi.org/10.1038/321599a0
931
932 Olu, K., 2014. PAMELA-MOZ01 cruise, L'Atalante R/V. https://doi.org/10.17600/14001000
933
934 O'Nions, R.K., Carter, S.R., Cohen, R.S., Evensen, N.M., Hamilton, P.J., 1978. Pb, Nd and Sr
935 isotopes in oceanic ferromanganese deposits and ocean floor basalts. Nature 273, 435–438.
936 https://doi.org/10.1038/273435a0
937
938 O'Nions, R.K., Frank, M., von Blanckenburg, F., Ling, H.-F., 1998. Secular variation of Nd
939 and Pb isotopes in ferromanganese crusts from the Atlantic, Indian and Pacific Oceans. Earth
940 Planet. Sci. Lett. 155, 15–28. https://doi.org/10.1016/S0012-821X(97)00207-0
941
942 Paquette, J.-L., Nédélec, A., Moine, B., Rakotondrazafy, M., 1994. U-Pb, Single Zircon Pb-
943 Evaporation, and Sm-Nd Isotopic Study of a Granulite Domain in SE Madagascar. J. Geol.
944 102, 523–538. https://doi.org/10.1086/629696
945
946 Pearce, C.R., Jones, M.T., Oelkers, E.H., Pradoux, C., Jeandel, C., 2013. The effect of
947 particulate dissolution on the neodymium (Nd) isotope and Rare Earth Element (REE)
948 composition of seawater. Earth Planet. Sci. Lett. 369–370, 138–147.
949 https://doi.org/10.1016/j.epsl.2013.03.023
950
951 Piepgras, D.J., Jacobsen, S.B., 1988. The isotopic composition of neodymium in the North
952 Pacific. Geochim. Cosmochim. Acta 52, 1373–1381. https://doi.org/10.1016/0016-
953 7037(88)90208-6

954

955 Piepgras, D.J., Wasserburg, G.J., 1987. Rare earth element transport in the western North
956 Atlantic inferred from Nd isotopic observations. Geochim. Cosmochim. Acta 51, 1257–1271.
957 https://doi.org/10.1016/0016-7037(87)90217-1

958

959 Piepgras, D.J., Wasserburg, G.J., 1982. Isotopic Composition of Neodymium in Waters from
960 the Drake Passage. Science 217, 207–214.

961

962 Piepgras, D.J., Wasserburg, G.J., 1980. Neodymium isotopic variations in seawater. Earth
963 Planet. Sci. Lett. 50, 128–138. https://doi.org/10.1016/0012-821X(80)90124-7

964

965 Piepgras, D.J., Wasserburg, G.J., Dasch, E.J., 1979. The isotopic composition of Nd in
966 different ocean masses. Earth Planet. Sci. Lett. 45, 223–236. https://doi.org/10.1016/0012-
967 821X(79)90125-0

968

969 Pin, C., Briot, D., Bassin, C., Poitrasson, F., 1994. Concomitant separation of strontium and
970 samarium-neodymium for isotopic analysis in silicate samples, based on specific extraction
971 chromatography. Anal. Chim. Acta 298, 209–217. https://doi.org/10.1016/0003-
972 2670(94)00274-6

973

974 Piotrowski, A.M., Banakar, V.K., Scrivner, A.E., Elderfield, H., Galy, A., Dennis, A., 2009.
975 Indian Ocean circulation and productivity during the last glacial cycle. Earth Planet. Sci. Lett.
976 285, 179–189. https://doi.org/10.1016/j.epsl.2009.06.007

977

978 Piotrowski, A.M., Galy, A., Nicholl, J.A.L., Roberts, N., Wilson, D.J., Clegg, J.A., Yu, J.,
979 2012. Reconstructing deglacial North and South Atlantic deep water sourcing using
980 foraminiferal Nd isotopes. Earth Planet. Sci. Lett. 357–358, 289–297.
981 https://doi.org/10.1016/j.epsl.2012.09.036
982
983 Piotrowski, A.M., Goldstein, S.L., Hemming, S.R., Fairbanks, R.G., 2005. Temporal
984 Relationships of Carbon Cycling and Ocean Circulation at Glacial Boundaries. Science 307,
985 1933–1938. https://doi.org/10.1126/science.1104883
986
987 Piotrowski, A.M., Goldstein, S.L., Hemming, S.R., Fairbanks, R.G., 2004. Intensification and
988 variability of ocean thermohaline circulation through the last deglaciation. Earth Planet. Sci.
989 Lett. 225, 205–220. https://doi.org/10.1016/j.epsl.2004.06.002
990
991 Piper, D.Z., 1974. Rare earth elements in ferromanganese nodules and other marine phases.
992 Geochim. Cosmochim. Acta 38, 1007–1022. https://doi.org/10.1016/0016-7037(74)90002-7
993
994 Puteanus, D., Halbach, P., 1988. Correlation of Co concentration and growth rate — A
995 method for age determination of ferromanganese crusts. Chem. Geol. 69, 73–85.
996 https://doi.org/10.1016/0009-2541(88)90159-3
997
998 Quartly, G.D., de Cuevas, B.A., Coward, A.C., 2013. Mozambique Channel eddies in GCMs:
999 A question of resolution and slippage. Ocean Model. 63, 56–67.
1000 https://doi.org/10.1016/j.ocemod.2012.12.011
1001

Rahlf, P., Hathorne, E., Laukert, G., Gutjahr, M., Weldeab, S., Frank, M., 2020. Tracing water mass mixing and continental inputs in the southeastern Atlantic Ocean with dissolved neodymium isotopes. Earth Planet. Sci. Lett. 530, 115944. https://doi.org/10.1016/j.epsl.2019.115944

Rempfer, J., Stocker, T.F., Joos, F., Dutay, J.-C., Siddall, M., 2011. Modelling Nd-isotopes with a coarse resolution ocean circulation model: Sensitivities to model parameters and source/sink distributions. Geochim. Cosmochim. Acta 75, 5927–5950. https://doi.org/10.1016/j.gca.2011.07.044

Rickli, J., Frank, M., Baker, A.R., Aciego, S., de Souza, G., Georg, R.B., Halliday, A.N., 2010. Hafnium and neodymium isotopes in surface waters of the eastern Atlantic Ocean: Implications for sources and inputs of trace metals to the ocean. Geochim. Cosmochim. Acta 74, 540–557. https://doi.org/10.1016/j.gca.2009.10.006

Rickli, J., Frank, M., Halliday, A.N., 2009. The hafnium–neodymium isotopic composition of Atlantic seawater. Earth Planet. Sci. Lett. 280, 118–127. https://doi.org/10.1016/j.epsl.2009.01.026

Roberts, N.L., Piotrowski, A.M., McManus, J.F., Keigwin, L.D., 2010. Synchronous Deglacial Overturning and Water Mass Source Changes. Science 327, 75–78. https://doi.org/10.1126/science.1178068

1025 Rogers, W.E., Hartman, W.D., Krause, K.S.K., 2000. Stratigraphic Analysis of Upper
1026 Cretaceous Rocks in the Mahajanga Basin, Northwestern Madagascar: Implications for
1027 Ancient and Modern Faunas. J. Geol. 108, 275–301.
1028
1029 Rutberg, R.L., Hemming, S.R., Goldstein, S.L., 2000. Reduced North Atlantic Deep Water
1030 flux to the glacial Southern Ocean inferred from neodymium isotope ratios. Nature 405, 935.
1031 https://doi.org/10.1038/35016049
1032
1033 Schacht, U., Wallmann, K., Kutterolf, S., 2010. The influence of volcanic ash alteration on
1034 the REE composition of marine pore waters. J. Geochem. Explor., GEOFLUIDS VI: Recent
1035 Advances in Research on Fluids in Geological Processes 106, 176–187.
1036 https://doi.org/10.1016/j.gexplo.2010.02.006
1037
1038 Schott, F.A., McCreary, J.P., 2001. The monsoon circulation of the Indian Ocean. Prog.
1039 Oceanogr. 51, 1–123. https://doi.org/10.1016/S0079-6611(01)00083-0
1040
1041 Segl, M., Mangini, A., Bonani, G., Hofmann, H.J., Nessi, M., Suter, M., Wölfli, W.,
1042 Friedrich, G., Plüger, W.L., Wiechowski, A., Beer, J., 1984. 10 Be-dating of a manganese
1043 crust from Central North Pacific and implications for ocean palaeocirculation. Nature 309,
1044 540. https://doi.org/10.1038/309540a0
1045
1046 Shimizu, H., Tachikawa, K., Masuda, A., Nozaki, Y., 1994. Cerium and neodymium isotope
1047 ratios and REE patterns in seawater from the North Pacific Ocean. Geochim. Cosmochim.
1048 Acta 58, 323–333. https://doi.org/10.1016/0016-7037(94)90467-7
1049

Stichel, T., Frank, M., Rickli, J., Haley, B.A., 2012a. The hafnium and neodymium isotope composition of seawater in the Atlantic sector of the Southern Ocean. Earth Planet. Sci. Lett. 317–318, 282–294. https://doi.org/10.1016/j.epsl.2011.11.025

Stichel, T., Frank, M., Rickli, J., Hathorne, E.C., Haley, B.A., Jeandel, C., Pradoux, C., 2012b. Sources and input mechanisms of hafnium and neodymium in surface waters of the Atlantic sector of the Southern Ocean. Geochim. Cosmochim. Acta 94, 22–37. https://doi.org/10.1016/j.gca.2012.07.005

Storey, M., Mahoney, J.J., Saunders, A.D., Duncan, R.A., Kelley, S.P., Coffin, M.F., 1995. Timing of Hot Spot—Related Volcanism and the Breakup of Madagascar and India. Science 267, 852–855. https://doi.org/10.1126/science.267.5199.852

Tachikawa, K., Arsouze, T., Bayon, G., Bory, A., Colin, C., Dutay, J.-C., Frank, N., Giraud, X., Gourlan, A.T., Jeandel, C., Lacan, F., Meynadier, L., Montagna, P., Piotrowski, A.M., Plancherel, Y., Pucéat, E., Roy-Barman, M., Waelbroeck, C., 2017. The large-scale evolution of neodymium isotopic composition in the global modern and Holocene ocean revealed from seawater and archive data. Chem. Geol. 457, 131–148. https://doi.org/10.1016/j.chemgeo.2017.03.018

Tachikawa, K., Athias, V., Jeandel, C., 2003. Neodymium budget in the modern ocean and paleo-oceanographic implications. J. Geophys. Res. Oceans 108. https://doi.org/10.1029/1999JC000285

Tachikawa, K., Handel, C., Dupré, B., 1997. Distribution of rare earth elements and neodymium isotopes in settling particulate material of the tropical Atlantic Ocean (EUMELI site). Deep Sea Res. Part Oceanogr. Res. Pap. 44, 1769–1792. https://doi.org/10.1016/S0967-0637(97)00057-5

Tanaka, T., Togashi, S., Kamioka, H., Amakawa, H., Kagami, H., Hamamoto, T., Yuhara, M., Orihashi, Y., Yoneda, S., Shimizu, H., Kunimaru, T., Takahashi, K., Yanagi, T., Nakano, T., Fujimaki, H., Shinjo, R., Asahara, Y., Tanimizu, M., Dragusanu, C., 2000. JNdi-1: a neodymium isotopic reference in consistency with LaJolla neodymium. Chem. Geol. 168, 279–281. https://doi.org/10.1016/S0009-2541(00)00198-4

Thompson, J.O., Moulin, M., Aslanian, D., de Clarens, P., Guillocheau, F., 2019. New starting point for the Indian Ocean: Second phase of breakup for Gondwana. Earth-Sci. Rev. 191, 26–56. https://doi.org/10.1016/j.earscirev.2019.01.018

Toole, J.M., Warren, B.A., 1993. A hydrographic section across the subtropical South Indian Ocean. Deep Sea Res. Part Oceanogr. Res. Pap. 40, 1973–2019. https://doi.org/10.1016/0967-0637(93)90042-2

Torsvik, T.H., Tucker, R.D., Ashwal, L.D., Carter, L.M., Jamtveit, B., Vidyadharan, K.T., Venkataramana, P., 2000. Late Cretaceous India-Madagascar fit and timing of break-up related magmatism. Terra Nova 12, 220–224. https://doi.org/10.1046/j.1365-3121.2000.00300.x

1098 Ullgren, J.E., van Aken, H.M., Ridderinkhof, H., de Ruijter, W.P.M., 2012. The hydrography
1099 of the Mozambique Channel from six years of continuous temperature, salinity, and velocity
1100 observations. Deep Sea Res. Part Oceanogr. Res. Pap. 69, 36–50.
1101 https://doi.org/10.1016/j.dsr.2012.07.003
1102
1103 van Aken, H.M., Ridderinkhof, H., de Ruijter, W.P.M., 2004. North Atlantic deep water in the
1104 south-western Indian Ocean. Deep Sea Res. Part Oceanogr. Res. Pap. 51, 755–776.
1105 https://doi.org/10.1016/j.dsr.2004.01.008
1106
1107 van der Lubbe, H.J.L., Frank, M., Tjallingii, R., Schneider, R.R., 2016. Neodymium isotope
1108 constraints on provenance, dispersal, and climate-driven supply of Zambezi sediments along
1109 the Mozambique Margin during the past ~45,000 years. Geochem. Geophys. Geosystems 17,
1110 181–198. https://doi.org/10.1002/2015GC006080
1111
1112 Wei, R., Abouchami, W., Zahn, R., Masque, P., 2016. Deep circulation changes in the South
1113 Atlantic since the Last Glacial Maximum from Nd isotope and multi-proxy records. Earth
1114 Planet. Sci. Lett. 434, 18–29. https://doi.org/10.1016/j.epsl.2015.11.001
1115
1116 Weijer, W., 1999. Impact of Interbasin Exchange on the Atlantic Overturning Circulation. J.
1117 Phys. Oceanogr. 29, 19.
1118
1119 Wilson, D.J., Piotrowski, A.M., Galy, A., McCave, I.N., 2012. A boundary exchange
1120 influence on deglacial neodymium isotope records from the deep western Indian Ocean. Earth
1121 Planet. Sci. Lett. 341–344, 35–47. https://doi.org/10.1016/j.epsl.2012.06.009
1122

1123 You, Y., 2000. Implications of the deep circulation and ventilation of the Indian Ocean on the
1124 renewal mechanism of North Atlantic Deep Water. J. Geophys. Res. Oceans 105, 23895–
1125 23926. https://doi.org/10.1029/2000JC900105
1126
1127 Yu, J., Elderfield, H., Piotrowski, A.M., 2008. Seawater carbonate ion-δ13C systematics and
1128 application to glacial–interglacial North Atlantic ocean circulation. Earth Planet. Sci. Lett.
1129 271, 209–220. https://doi.org/10.1016/j.epsl.2008.04.010

Figures and tables

Figure 1. (A) Bathymetry of the Mozambique Channel (data from GEBCO and PAMELA cruises) with its main structures including the Davie Ridge and the Eparses Islands. The white dots represent the dredging operations. (B) Bathymetry of the Mozambique Channel (data from GEBCO and PAMELA cruises) showing the main circulation patterns (based on Kolla et al., 1980; Fine, 1983; Toole and Warren, 1993; DiMarco et al., 2002; Lutjerharms, 2006; Ullgren et al., 2012). AABW: Antarctic Bottom Water; AAIW: Antarctic Intermediate Water; AC: Agulhas Current; AUC: Agulhas Undercurrent; MC: Mozambique Current; ME: Mozambique Eddies; MUC: Mozambique Undercurrent; NADW: North Atlantic Deep Water; NIDW: North Indian Deep Water; RSW: Red Sea Water; SW: Surface Water including TSW: Tropical Surface Water, STSW: Sub-Tropical Surface Water and SICW: South Indian Central Water. The dark line corresponds to the section located in 1C. Nd isotope signatures (ε_{Nd}) are presented for the main geological formations surrounding the channel (ε_{Nd} of Archean basement : Paquette et al., 1994; Jelsma et al., 1996; Möller et al., 1998; Kröner et al., 2000; De Waele, 2006; Grantham et al., 2011 and ε_{Nd} of the volcanic structures : Mahoney et al., 1991; Grousset et al., 1992; Jourdan et al., 2007). (C) Salinity section showing the distribution of the main water masses present in the Mozambique Channel, based on Conductivity Temperature Depth (CTD) profiles.

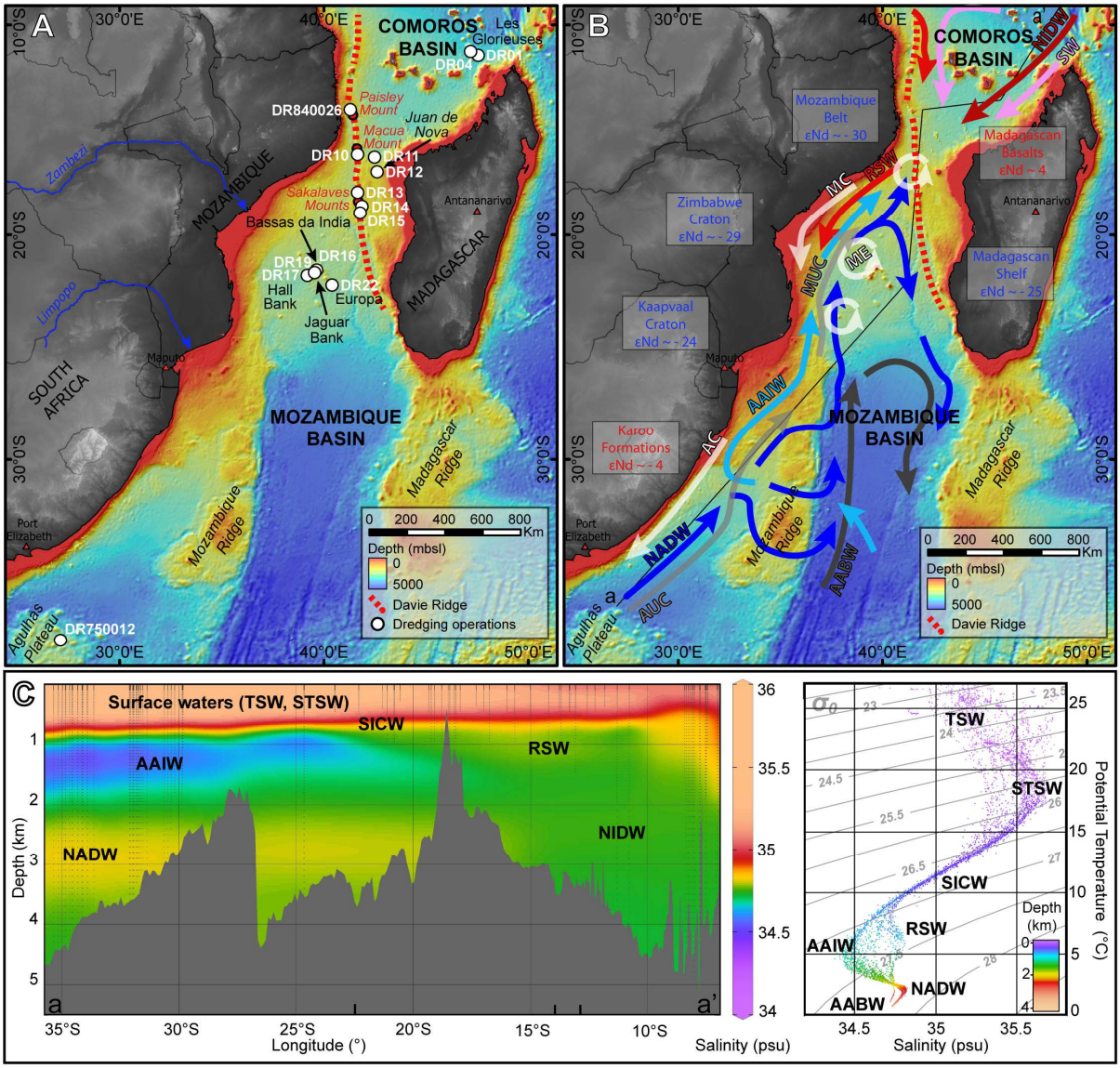
A
B
C
COMOROS BASIN
Les Glorieuses
DR01
DR04
DR840026
Paisley Mount
Juan de Nova
Macua Mount
DR10
DR11
DR12
Sakalaves Mounts
DR13
DR14
DR15
Bassas da India
DR16
DR17
DR19
Hall Bank
DR22
Europa
Jaguar Bank
DR750012
Zambezi
Limpopo
MOZAMBIQUE
SOUTH AFRICA
Maputo
Antananarivo
MADAGASCAR
MOZAMBIQUE BASIN
Madagascar Ridge
Mozambique Ridge
Port Elizabeth
Agulhas Plateau
Depth (mbsl)
0
5000
Davie Ridge
Dredging operations
Km
Mozambique Belt
εNd ~ - 30
Madagascan Basalts
εNd ~ 4
Zimbabwe Craton
εNd ~ - 29
Madagascan Shelf
εNd ~ - 25
Kaapvaal Craton
εNd ~ - 24
Karoo Formations
εNd ~ - 4
NIDW
SW
MC
RSW
MUC
ME
AAIW
AC
NADW
AUC
AABW
Surface waters (TSW, STSW)
SICW
RSW
AAIW
NIDW
NADW
Depth (km)
Longitude (°)
Salinity (psu)
Potential Temperature (°C)
TSW
STSW
SICW
RSW
AAIW
NADW
AABW

1148

1149 **Table 1.** Water masses abbreviations used in this study together with their corresponding

1150 depth range and ε_{Nd} signatures.

Abbreviations	Water masses	Depth range (mbsl)	εNd
SICW	South Indian Central Water	200-700	-8.5 to -7[a]
RSW	Red Sea Water	800-1400	-8.5 to -7[a]
AAIW	Antarctic Intermediate Water	800-1500	-9 to -8[b]
NIDW	North Indian Deep Water	2000-3000	-8.5 to -7[a]
NADW	North Atlantic Deep Water	1500-3500	-13 to -9[c]

1151 [a] Bertram and Elderfield (1993), Arsouze et al. (2007)

1152 [b] Piepgras and Wasserburg (1982), Jeandel (1993), Arsouze et al. (2007), Amakawa et al. (2013)

1153 [c] Piepgras and Wasserburg (1987), Jeandel (1993), Rickli et al. (2009), Tachikawa et al. (2017)

1154

1155 **Table 2.** International Geo Sample Number (IGSN), location, depth and ε_{Nd} values of the studied Fe-Mn crusts from the PAMELA-MOZ1 (Olu,

1156 2014), NOSICAA-MD06 (Leclaire, 1975) and RIDA-MD39 (Leclaire, 1984) oceanographic expeditions.

Cruise	Dredge	Sample	IGSN	Location	Latitude	Longitude	Depth range (mbsl)	$^{143}Nd/^{144}Nd$	2σ (10^{-6})	εNd	Percent NADW[b]
PAMELA-MOZ1											
	DR01	MOZ1-DR01-01	BFBG-155073	Glorieuses Islands	11°47'S	47°54'E	2400-2650	0.512255	4	-7.5	21-39
	DR04	MOZ1-DR04-01	BFBG-155082	Glorieuses Islands	11°28'S	47°32'E	1780-2000	0.512225	8	-8.1	29-45
	DR04	MOZ1-DR04-03	BFBG-155084	Glorieuses Islands	11°28'S	47°32'E	1780-2000	0.512227	8	-8.0	29-45
	DR04	MOZ1-DR04-04	BFBG-155085	Glorieuses Islands	11°28'S	47°32'E	1780-2000	0.512218	6	-8.2	31-47
	DR04	MOZ1-DR04-23	BFBG-169883	Glorieuses Islands	11°28'S	47°32'E	1780-2000	0.512208	4	-8.4	34-49
	DR10	MOZ1-DR10-04	BFBG-155152	Macua Mount	16°12'S	41°38'E	1000-1400	0.512226	4	-8.0	29-45
	DR10	MOZ1-DR10-05	BFBG-155153	Macua Mount	16°12'S	41°38'E	1000-1400	0.512237	6	-7.8	26-42
	DR11	MOZ1-DR11-01	BFBG-155160	Jeffrey Ridge	16°10'S	42°30'E	2400-2450	0.512180	4	-8.9	42-55
	DR11	MOZ1-DR11-03	BFBG-155162	Jeffrey Ridge	16°10'S	42°30'E	2400-2450	0.512191	4	-8.7	39-52
	DR11	MOZ1-DR11-05	BFBG-155164	Jeffrey Ridge	16°10'S	42°30'E	2400-2450	0.512197	4	-8.6	37-51
	DR11	MOZ1-DR11-07	BFBG-155166	Jeffrey Ridge	16°10'S	42°30'E	2400-2450	0.512157	8	-9.4	48-60
	DR12	MOZ1-DR12-09	BFBG-155179	Juan de Nova	17°1'S	42°36'E	1350-1650	0.512231	8	-7.9	28-44

DR12	MOZ1-DR12-14	BFBG-155184	Juan de Nova	17°1'S	42°36'E	1350-1650	0.512245	6	-7.7	24-41
DR12	MOZ1-DR12-V	BFBG-169884	Juan de Nova	17°1'S	42°36'E	1350-1650	0.512232	4	-7.9	27-44
DR13	MOZ1-DR13-07	BFBG-155191	North Sakalaves Mounts	17°59'S	41°39'E	1300-1600	0.512202	6	-8.5	36-50
DR14	MOZ1-DR14-04	BFBG-155201	Sakalaves Mounts	18°39'S	41°51'E	580-650	0.512249	4	-7.6	23-40
DR15	MOZ1-DR15-10	BFBG-155211	South Sakalaves Mounts	18°57'S	41°45'E	1200-1250	0.512236	4	-7.8	26-43
DR15	MOZ1-DR15-14	BFBG-155215	South Sakalaves Mounts	18°57'S	41°45'E	1200-1250	0.512247	8	-7.6	23-40
DR16	MOZ1-DR16-05	BFBG-155220	Bassas da India	21°36'S	39°38'E	1350-1600	0.512195	4	-8.6	38-51
DR16	MOZ1-DR16-06	BFBG-155221	Bassas da India	21°36'S	39°38'E	1350-1600	0.512172	4	-9.1	44-57
DR17	MOZ1-DR17-01	BFBG-155224	Hall Bank	21°50'S	39°10'E	1700-1900	0.512158	6	-9.4	48-60
DR17	MOZ1-DR17-04	BFBG-155227	Hall Bank	21°50'S	39°10'E	1700-1900	0.512175	6	-9.0	43-56
DR19	MOZ1-DR19-01	BFBG-155233	Jaguar Bank	21°44'S	39°32'E	1000-1350	0.512257	24	-7.4	20-38
DR22	MOZ1-DR22-01	BFBG-155243	Europa	21°18'S	40°23'E	1400-1550	0.512216	4	-8.2	32-47
DR22	MOZ1-DR22-02	BFBG-155244	Europa	21°18'S	40°23'E	1400-1550	0.512194	6	-8.7	38-52
DR22	MOZ1-DR22-03	BFBG-155245	Europa	21°18'S	40°23'E	1400-1550	0.512240	8	-7.8	25-42
DR22	MOZ1-DR22-06	BFBG-155248	Europa	21°18'S	40°23'E	1400-1550	0.512221	4	-8.1	30-46
RIDA-MD39										
DR84-0026	DR84-0026	MNHN-GS-DR84-0026	Paisley Mount	14°08'S	41°29'E	800-810	0.512272	4	-7.1	16-35

DR84-0026	DR84-02		Paisley Mount	14°08'S	41°29'E	800-810	0.512272	24	-7.4 [a]	20-38
DR84-0033	DR84-09		Macua Mount	16°12'S	41°39'E	700-953	0.512274	20	-7.1 [a]	16-35
NOSICAA-MD06										
DR75-0012	DR75-0012	MNHN-GS-DR75-0012	Agulhas Plateau	37°32'S	27°00'E	2550-2550	0.512119	6	-10.1	60-68
DR75-0012	DR75-08		Agulhas Plateau	37°32'S	27°00'E	2550-2550	0.512094	26	-10.6 [a]	66-73

[a] Albarède et al. (1997)

[b] Numbers are percentages of NADW calculated with Pacific water mass end-member values of ε_{Nd} = -4 and -6 (Frank et al., 2002)

Figure 2. Plot comparing ε_{Nd} data obtained from surface layer of Fe-Mn crusts (this study; white points) to ε_{Nd} values from the region. The yellow diamonds represent ε_{Nd} data from Zambezi sediments along the Mozambique Margin (van der Lubbe et al., 2016); the grey triangles show ε_{Nd} values from uncleaned foraminiferal coatings from the Madagascar Basin and Mascarene Basin (Wilson et al., 2012) and the blue points correspond to ε_{Nd} data from Fe-Mn nodules (Albarède et al., 1997). Seawater ε_{Nd} profiles are represented in green, orange and red respectively from the Madagascar Basin (CD1504/CD1505), the Somali Basin (CD1506/CD1507) and the Mascarene Basin (CD1502/CD1503; Bertram and Elderfield, 1993). Error bars on the data points represent 2σ. The grey arrow represents the Nd isotope variation of Wilson et al. (2012) study linked to unradiogenic Nd inputs along the Madagascan margin, whereas the black arrow corresponds to the trend of our study showing the opposite of that expected with a boundary exchange along an unradiogenic shelf. Black dotted lines and labels show the western Indian Ocean water column structure. Red dotted line corresponds to the average water depth of 1500 mbsl considered to separate intermediate and deep layers.

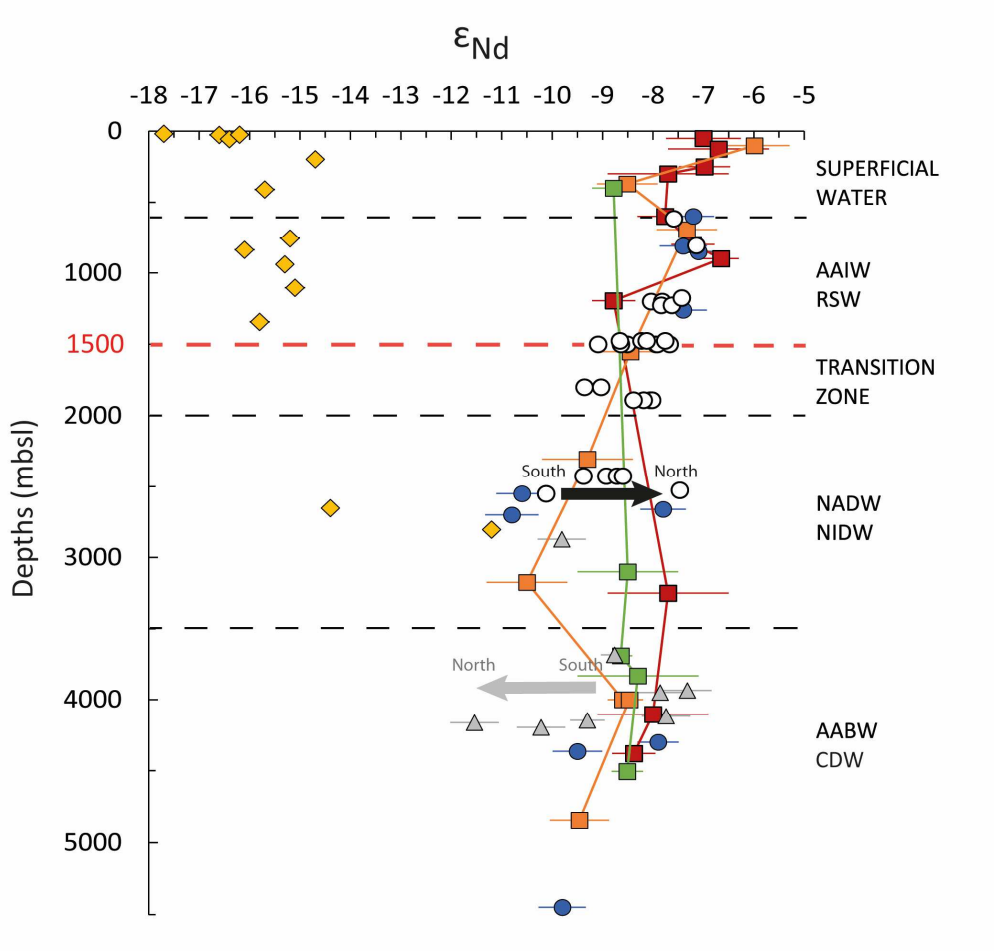
εNd
-18 -17 -16 -15 -14 -13 -12 -11 -10 -9 -8 -7 -6 -5
0
1000
1500
2000
3000
4000
5000
Depths (mbsl)
SUPERFICIAL WATER
AAIW
RSW
TRANSITION ZONE
NADW
NIDW
AABW
CDW
South
North
North
South

1174

Figure 3. (A) Bathymetry of the Mozambique Channel (data from GEBCO and PAMELA cruises) with ε_{Nd} values of the samples located above 1500 mbsl. (B) Bathymetry of the Mozambique Channel (data from GEBCO and PAMELA cruises) showing ε_{Nd} values of the samples located below 1500 mbsl. "n" represents the number of samples analysed per dredge.

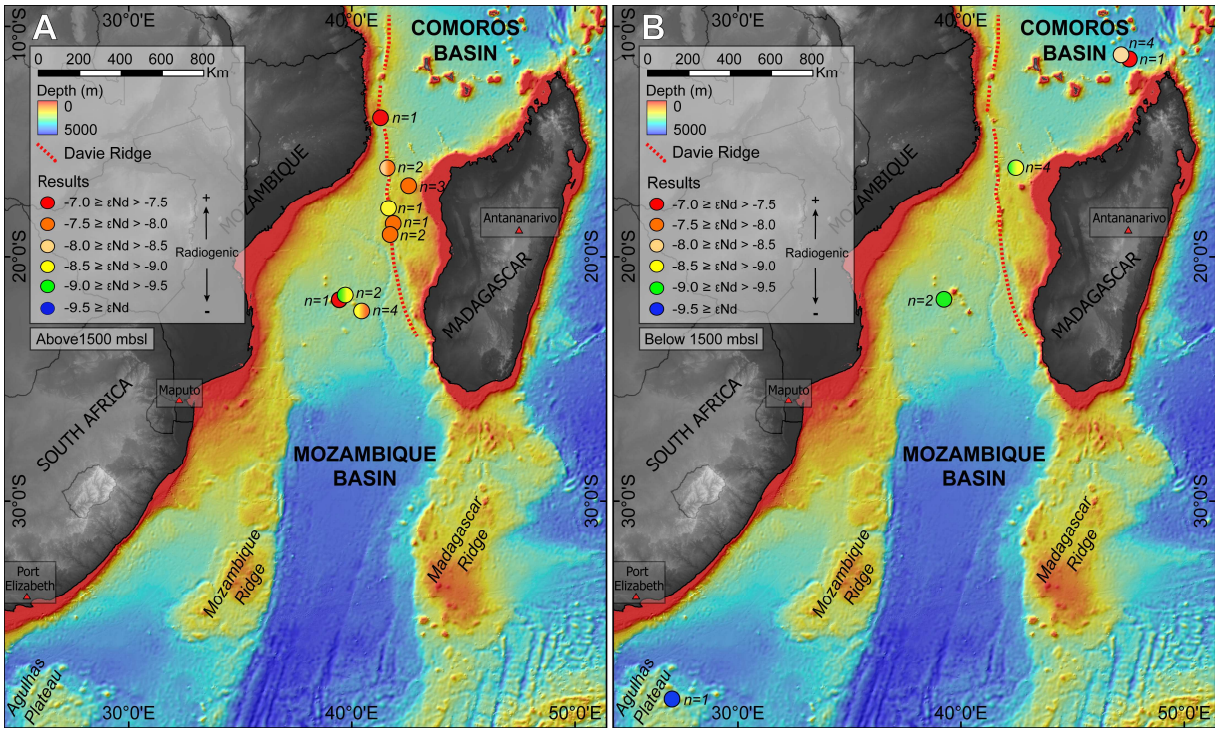

Figure 4. Bathymetry of the Mozambique Channel (data from GEBCO and PAMELA cruises) showing Atlantic waters contributions estimated through the Mozambique Channel (for Pacific ε_{Nd} = -6) and the resulting circulation of NADW. The dashed arrows present a suggestion of potential NADW passages beyond the Davie Ridge.

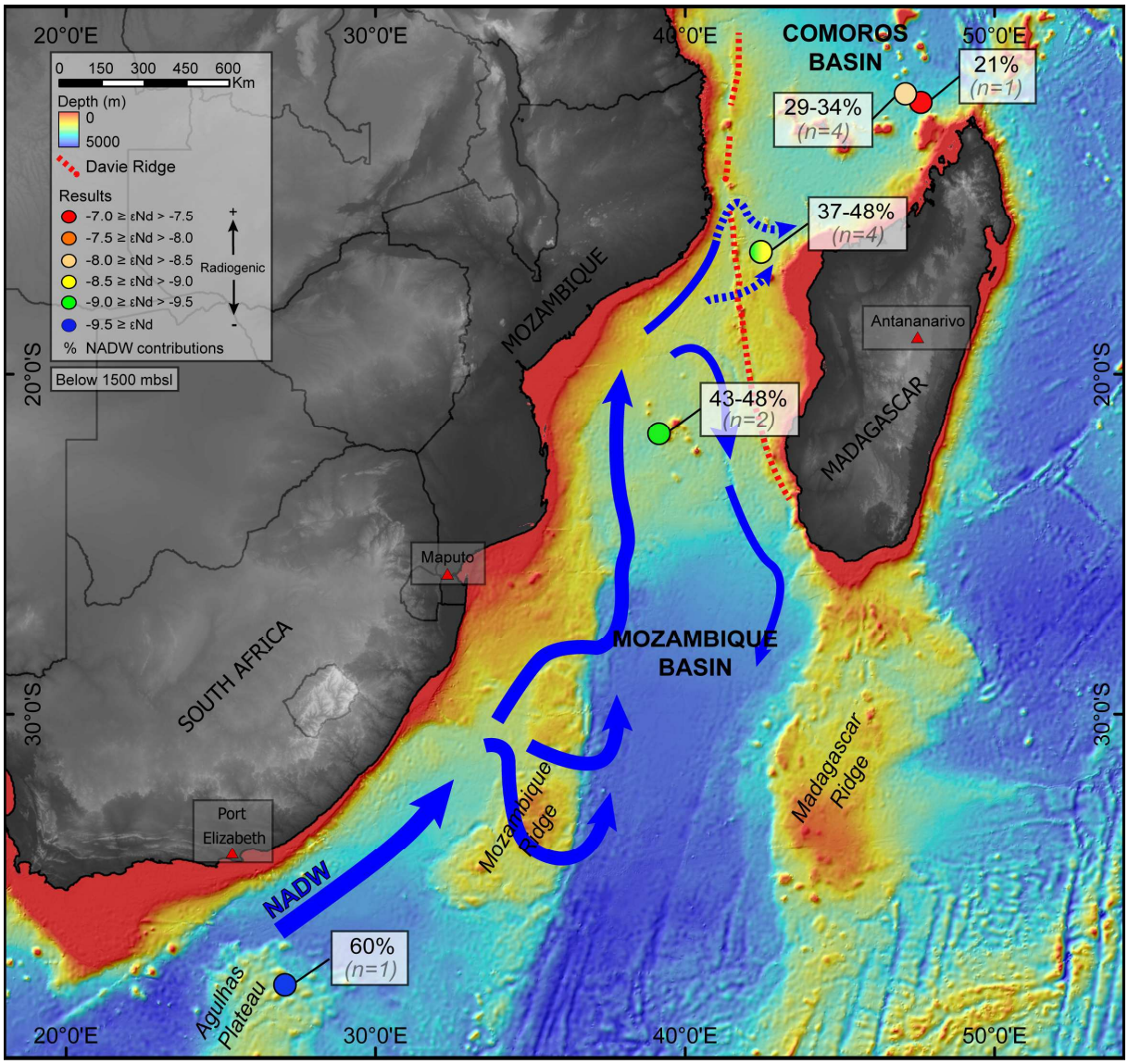

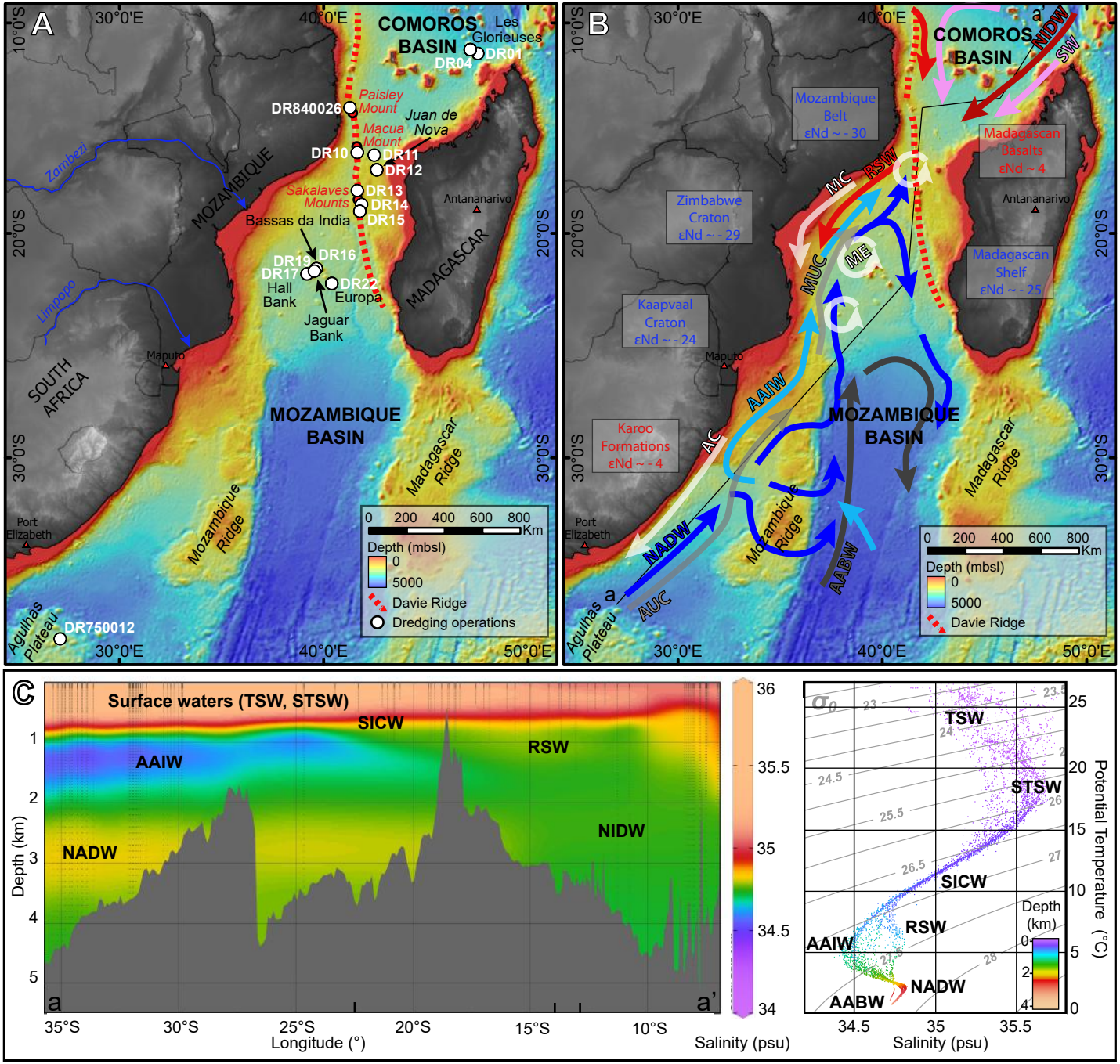
A
B
C
COMOROS BASIN
Les Glorieuses
DR01
DR04
DR840026
Paisley Mount
Juan de Nova
Macua Mount
DR10
DR11
DR12
Sakalaves Mounts
DR13
DR14
DR15
Bassas da India
DR16
DR19
DR17
DR22
Hall Bank
Europa
Jaguar Bank
DR750012
MOZAMBIQUE
MADAGASCAR
SOUTH AFRICA
Zambezi
Limpopo
Antananarivo
Maputo
Port Elizabeth
Agulhas Plateau
MOZAMBIQUE BASIN
Madagascar Ridge
Mozambique Ridge
Davie Ridge
Dredging operations
Depth (mbsl)
0
5000
0 200 400 600 800 Km
Mozambique Belt
εNd ~ - 30
Madagascan Basalts
εNd ~ 4
Zimbabwe Craton
εNd ~ - 29
Madagascan Shelf
εNd ~ - 25
Kaapvaal Craton
εNd ~ - 24
Karoo Formations
εNd ~ - 4
NIDW
SW
MC
RSW
MUC
ME
AAIW
AC
NADW
AUC
AABW
a
a'
Surface waters (TSW, STSW)
SICW
AAIW
RSW
NIDW
NADW
Depth (km)
Longitude (°)
Salinity (psu)
Potential Temperature (°C)
TSW
STSW
SICW
RSW
AAIW
NADW
AABW

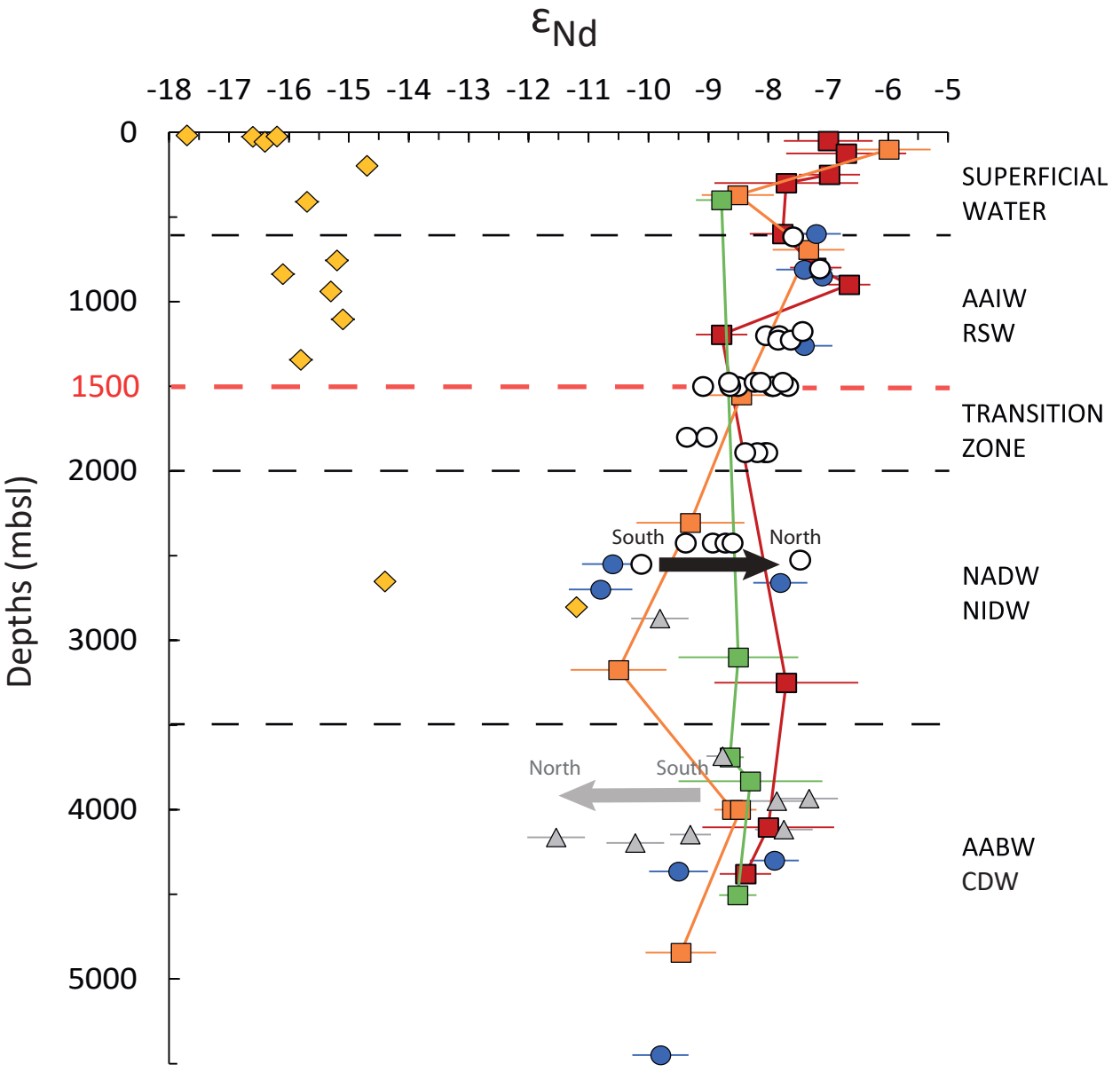
εNd
-18 -17 -16 -15 -14 -13 -12 -11 -10 -9 -8 -7 -6 -5
0
1000
1500
2000
3000
4000
5000
Depths (mbsl)
SUPERFICIAL WATER
AAIW
RSW
TRANSITION ZONE
NADW
NIDW
AABW
CDW
South
North
North
South

A

0 200 400 600 800 Km

Depth (m)
0
5000

Davie Ridge

Results
-7.0 ≥ εNd > -7.5
-7.5 ≥ εNd > -8.0
-8.0 ≥ εNd > -8.5
-8.5 ≥ εNd > -9.0
-9.0 ≥ εNd > -9.5
-9.5 ≥ εNd

+ Radiogenic -

Above1500 mbsl

n=1
n=2
n=3
n=1
n=1
n=2
n=1
n=2
n=4

COMOROS BASIN
MOZAMBIQUE BASIN
MOZAMBIQUE
MADAGASCAR
SOUTH AFRICA
Antananarivo
Maputo
Port Elizabeth
Mozambique Ridge
Madagascar Ridge
Agulhas Plateau

10°0'S
20°0'S
30°0'S
30°0'E
40°0'E
50°0'E

B

0 200 400 600 800 Km

Depth (m)
0
5000

Davie Ridge

Results
-7.0 ≥ εNd > -7.5
-7.5 ≥ εNd > -8.0
-8.0 ≥ εNd > -8.5
-8.5 ≥ εNd > -9.0
-9.0 ≥ εNd > -9.5
-9.5 ≥ εNd

+ Radiogenic -

Below 1500 mbsl

n=4
n=1
n=4
n=2
n=1

COMOROS BASIN
MOZAMBIQUE BASIN
MOZAMBIQUE
MADAGASCAR
SOUTH AFRICA
Antananarivo
Maputo
Port Elizabeth
Mozambique Ridge
Madagascar Ridge
Agulhas Plateau

10°0'S
20°0'S
30°0'S
30°0'E
40°0'E
50°0'E

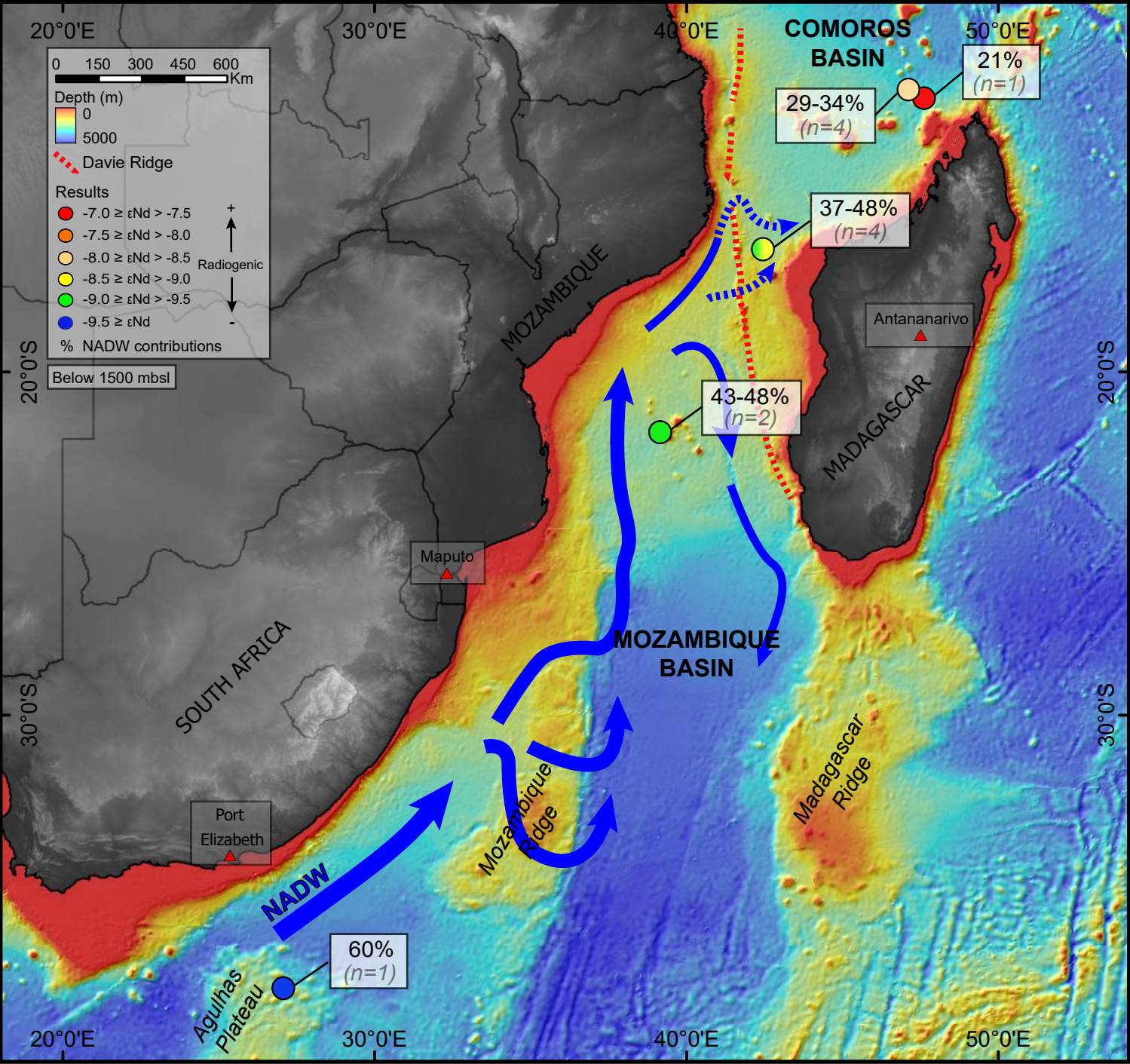
20°0'E
30°0'E
40°0'E
50°0'E
20°0'S
30°0'S
0 150 300 450 600
Km
Depth (m)
0
5000
Davie Ridge
Results
-7.0 ≥ εNd > -7.5
-7.5 ≥ εNd > -8.0
-8.0 ≥ εNd > -8.5
-8.5 ≥ εNd > -9.0
-9.0 ≥ εNd > -9.5
-9.5 ≥ εNd
+
Radiogenic
-
% NADW contributions
Below 1500 mbsl
COMOROS BASIN
21% (n=1)
29-34% (n=4)
37-48% (n=4)
43-48% (n=2)
MOZAMBIQUE
MADAGASCAR
Antananarivo
Maputo
SOUTH AFRICA
MOZAMBIQUE BASIN
Port Elizabeth
NADW
Mozambique Ridge
Madagascar Ridge
60% (n=1)
Agulhas Plateau

Abbreviations	Water masses	Depth range (mbsl)	εNd
SICW	South Indian Central Water	200-700	-8.5 to -7[a]
RSW	Red Sea Water	800-1400	-8.5 to -7[a]
AAIW	Antarctic Intermediate Water	800-1500	-9 to -8[b]
NIDW	North Indian Deep Water	2000-3000	-8.5 to -7[a]
NADW	North Atlantic Deep Water	1500-3500	-13 to -9[c]

[a] Bertram and Elderfield (1993), Arsouze et al. (2007)

[b] Piepgras and Wasserburg (1982), Jeandel (1993), Arsouze et al. (2007), Amakawa et al. (2013)

[c] Piepgras and Wasserburg (1987), Jeandel (1993), Rickli et al. (2009), Tachikawa et al. (2017)

Cruise	Dredge	Sample	IGSN	Location	Latitute	Longitude	Depth range (mbsl)	$^{143}Nd/^{144}Nd$	2σ (10^{-6})	εNd	Percent NADW [b]
PAMELA-MOZ-1	DR01	MOZ1-DR01-01	BFBG-155073	Glorieuses Islands	11°47'S	47°54'E	2400-2650	0.512255	4	-7.47	21-39
	DR04	MOZ1-DR04-01	BFBG-155082	Glorieuses Islands	11°28'S	47°32'E	1780-2000	0.512225	8	-8.1	29-45
	DR04	MOZ1-DR04-03	BFBG-155084	Glorieuses Islands	11°28'S	47°32'E	1780-2000	0.512227	8	-8.0	29-45
	DR04	MOZ1-DR04-04	BFBG-155085	Glorieuses Islands	11°28'S	47°32'E	1780-2000	0.512218	6	-8.2	31-47
	DR04	MOZ1-DR04-23	BFBG-169883	Glorieuses Islands	11°28'S	47°32'E	1780-2000	0.512208	4	-8.4	34-49
	DR10	MOZ1-DR10-04	BFBG-155152	Macua Mount	16°12'S	41°38'E	1000-1400	0.512226	4	-8.0	29-45
	DR10	MOZ1-DR10-05	BFBG-155153	Macua Mount	16°12'S	41°38'E	1000-1400	0.512237	6	-7.8	26-42
	DR11	MOZ1-DR11-01	BFBG-155160	Jeffrey Ridge	16°10'S	42°30'E	2400-2450	0.512180	4	-8.9	42-55
	DR11	MOZ1-DR11-03	BFBG-155162	Jeffrey Ridge	16°10'S	42°30'E	2400-2450	0.512191	4	-8.7	39-52
	DR11	MOZ1-DR11-05	BFBG-155164	Jeffrey Ridge	16°10'S	42°30'E	2400-2450	0.512197	4	-8.6	37-51
	DR11	MOZ1-DR11-07	BFBG-155166	Jeffrey Ridge	16°10'S	42°30'E	2400-2450	0.512157	8	-9.4	48-60
	DR12	MOZ1-DR12-09	BFBG-155179	Juan de Nova	17°1'S	42°36'E	1350-1650	0.512231	8	-7.9	28-44
	DR12	MOZ1-DR12-14	BFBG-155184	Juan de Nova	17°1'S	42°36'E	1350-1650	0.512245	6	-7.7	24-41
	DR12	MOZ1-DR12-V	BFBG-169884	Juan de Nova	17°1'S	42°36'E	1350-1650	0.512232	4	-7.9	27-44
	DR13	MOZ1-DR13-07	BFBG-155191	North Sakalaves Mounts	17°59'S	41°39'E	1300-1600	0.512202	6	-8.5	36-50
	DR14	MOZ1-DR14-04	BFBG-155201	Sakalaves Mounts	18°39'S	41°51'E	580-650	0.512249	4	-7.6	23-40
	DR15	MOZ1-DR15-10	BFBG-155211	South Sakalaves Mounts	18°57'S	41°45'E	1200-1250	0.512236	4	-7.8	26-43
	DR15	MOZ1-DR15-14	BFBG-155215	South Sakalaves Mounts	18°57'S	41°45'E	1200-1250	0.512247	8	-7.6	23-40
	DR16	MOZ1-DR16-05	BFBG-155220	Bassas da India	21°36'S	39°38'E	1350-1600	0.512195	4	-8.6	38-51
	DR16	MOZ1-DR16-06	BFBG-155221	Bassas da India	21°36'S	39°38'E	1350-1600	0.512172	4	-9.1	44-57
	DR17	MOZ1-DR17-01	BFBG-155224	Hall Bank	21°50'S	39°10'E	1700-1900	0.512158	6	-9.4	48-60
	DR17	MOZ1-DR17-04	BFBG-155227	Hall Bank	21°50'S	39°10'E	1700-1900	0.512175	6	-9.0	43-56
	DR19	MOZ1-DR19-01	BFBG-155233	Jaguar Bank	21°44'S	39°32'E	1000-1350	0.512257	24	-7.4	20-38
	DR22	MOZ1-DR22-01	BFBG-155243	Europa	21°18'S	40°23'E	1400-1550	0.512216	4	-8.2	32-47
	DR22	MOZ1-DR22-02	BFBG-155244	Europa	21°18'S	40°23'E	1400-1550	0.512194	6	-8.7	38-52
	DR22	MOZ1-DR22-03	BFBG-155245	Europa	21°18'S	40°23'E	1400-1550	0.512240	8	-7.8	25-42
	DR22	MOZ1-DR22-06	BFBG-155248	Europa	21°18'S	40°23'E	1400-1550	0.512221	4	-8.1	30-46
MD-39 Rida	DR84-0026	DR84-0026	MNHN-GS-DR84-0026	Paisley Mount	14°08'S	41°29'E	800-810	0.512272	4	-7.1	16-35
	DR84-0026	DR84-02		Paisley Mount	14°08'S	41°29'E	800-810	0.512272	24	-7.4 [a]	20-38
	DR84-0033	DR84-09		Macua Mount	16°12'S	41°39'E	700-953	0.512274	20	-7.1 [a]	16-35
MD-06 Nosicaa	DR75-0012	DR75-0012	MNHN-GS-DR75-0012	Agulhas Plateau	37°32'S	27°00'E	2550-2550	0.512119	6	-10.1	60-68
	DR75-0012	DR75-08		Agulhas Plateau	37°32'S	27°00'E	2550-2550	0.512094	26	-10.6 [a]	66-73

[a] Albarède et al. (1997)

[b] Numbers are percentages of NADW calculated with Pacific water mass end-member values of εNd = -4 and -6 (Frank et al., 2002)

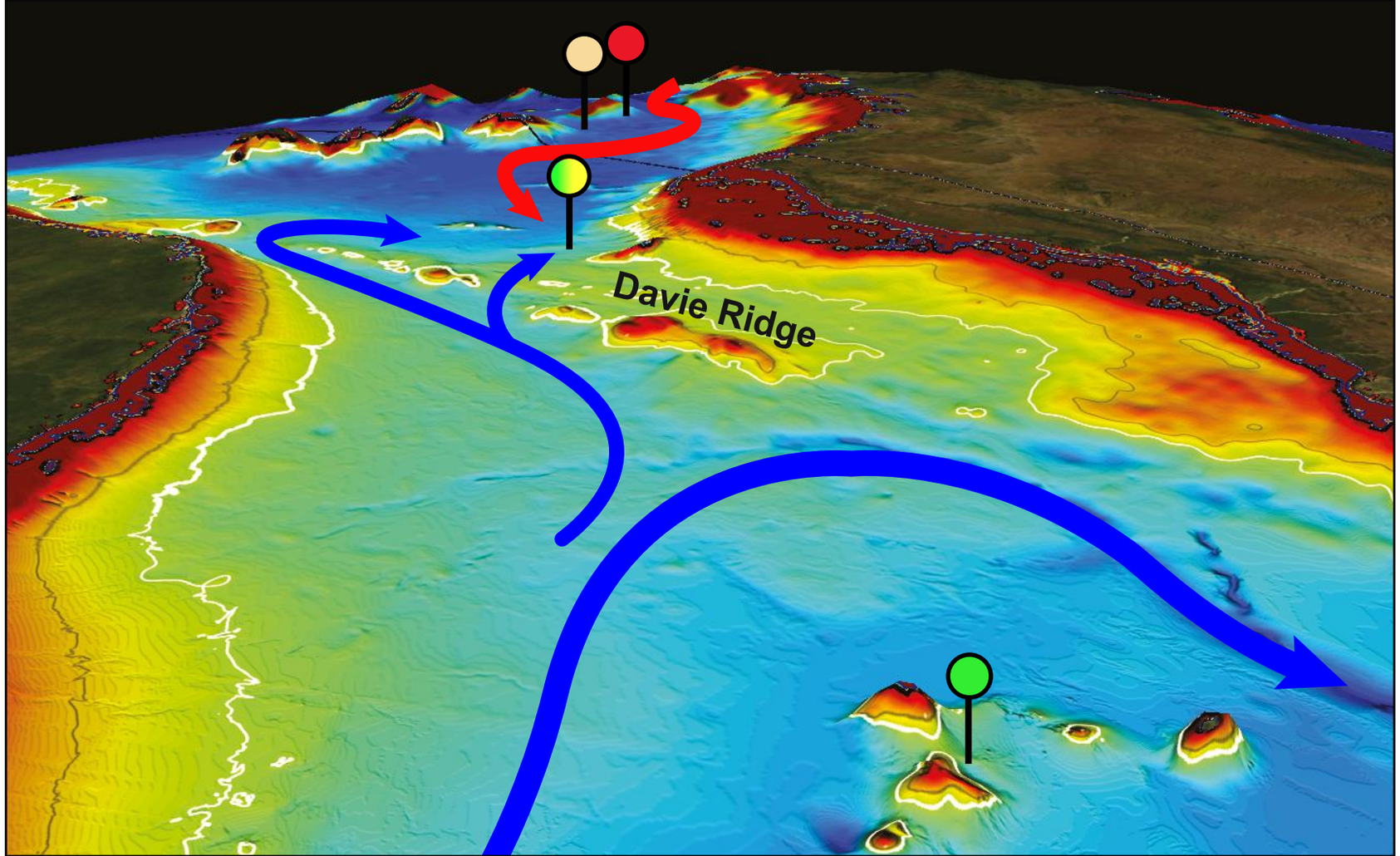

0 40 80 120 Km

Depth (m)

0

5000

Isocontours (m)

1500

2000

Values

-7.0 ≥ εNd > -7.5

-7.5 ≥ εNd > -8.0

-8.0 ≥ εNd > -8.5

-8.5 ≥ εNd > -9.0

-9.0 ≥ εNd > -9.5

-9.5 ≥ εNd

+

Radiogenic

-

North Atlantic Deep Water

North Indian Deep Water

Below 1500 mbsl